FEATURE ARTICLE

Dynamics of Insertion Reactions of H_2 Molecules with Excited Atoms

F. J. Aoiz* and L. Bañares

Departamento de Química Física, Facultad de Química, Universidad Complutense, 28040 Madrid, Spain

V. J. Herrero

Instituto de Estructura de la Materia (CSIC), Serrano 123, 28006 Madrid, Spain

Received: June 19, 2006; In Final Form: September 19, 2006

Recent progress in the study of insertion reactions of hydrogen molecules with excited atoms is reviewed in this article. In particular, the dynamics of the reaction of O(^1D), N(^2D), C(^1D), and S(^1D) with H_2 and its isotopomers, which have received a great deal of attention over the past decade, are examined in detail. All of these systems have in common the existence of several potential energy surfaces (PES) correlating with the reagents' states, and consequently, they can give rise to reaction following different adiabatic and nonadiabatic pathways. The main contribution, however, arises from their ground singlet PESs which feature the existence of deep wells with small or null barriers for insertion. Accordingly, these reactions proceed mainly via formation of relatively long-lived collision complexes and display an overall nearly statistical behavior. In spite of their similarities, the various reactions have peculiar characteristics caused by important differences of their respective PESs. The contribution of excited PES to the global reactivity, which has also become an important issue and a challenge both for theory and experiment, is also examined. The different theoretical approaches are discussed in the text, along with the experimental results obtained by a variety of techniques. The recent exact quantum treatments of these reactive systems together with the development of a rigorous statistical model have contributed to a very accurate description which in many cases matches very well the detailed measurements. The quasi−classical trajectory (QCT) method has also provided a fairly accurate description of the reaction dynamics for these systems. In particular, the analysis in terms of collision times has yielded interesting clues about the reaction mechanisms.

I. Introduction

Gas phase insertion reactions of H_2 molecules with excited atoms have been known for a long time. The photosensitization technique, used for the chemical activation of molecular bonds, was in fact started with the study of the Hg($^3P_1$) + H_2 → Hg + H + H reaction in the second decade of the 20th century.[1] In this early work, it was already suggested that the mercury atom should insert in the middle of the interatomic bond, rather than attack either of the molecular ends.

Reactions of excited metallic atoms with H_2, and with other H−X bonds, have been extensively studied since the 1970s by a variety of techniques and the results have been rationalized with considerations of orbital symmetry and steric requirements (see refs 2 and 3 and references therein). The prevalence of insertion mechanisms was established in these studies. Reactions of H_2 with other excited atoms, especially with O(^1D), also have a long research tradition in reaction dynamics.[4−6] After some initial debate, the available experimental data on cross-sections, rate coefficients, and products' states distributions were essentially interpreted, during the 1980s, in terms of a reaction mechanism involving the barrierless insertion of the O(^1D) atom into the H_2 bond, giving rise to a vibrationally excited water molecule in its ground electronic state, H_2O (1^1A_1), as a relatively short-lived reaction intermediate that would subsequently decay to OH + H (see the discussion in refs 7−9 for details).

In later times, reactions of molecular hydrogen with C(^1D), N(^2D), and S(^1D) have been also studied with increasing accuracy. All of these systems share with O(^1D) + H_2 the presence of a deep well in the potential energy surface (PES), associated with the corresponding AH_2 stable molecule or radical (H_2O, CH_2, NH_2, and H_2S), and proceeding mostly via an insertion mechanism, but each of them with dynamical peculiarities worth considering. In contrast to direct reactions, mostly of abstraction type, in which one bond is broken and another formed in a concerted, simultaneous way, in insertion reactions two bonds are formed, and only after a shorter or longer lapsus of time is one of them broken. Hence, they give rise to an intermediate species which can be considered as a superexcited molecule or radical. Besides their fundamental interest for the investigation of elementary processes, these reactions are relevant in different environments like atmospheric and astrophysical chemistry, combustion, and technological plasmas.

The study of these reactions posed a challenge from the theoretical point view, since they required a high level of

* To whom correspondence should be addressed. E-mail: aoiz@quim.ucm.es.

10.1021/jp063815o CCC: $33.50
Published on Web 11/16/2006

F. Javier Aoiz received his B.S. degree in Chemistry in 1976 from Universidad Complutense de Madrid, Spain and his Ph.D. from that same university in 1981. He spent a two year periond at Columbia University as a Fulbright fellow, working with the late Professor R. B. Bernstein. He joined the faculty of the Physical Chemistry Department at Universidad Complutense de Madrid in 1984 as an Associate Professor and got a chair in Physical Chemistry as a full Professor in 1999. He has been a visiting Professor at the University of Oxford (U.K.) and UCLA (CA, U.S.A.). His research activities are related to experimental and theoretical chemical reaction dynamics and photodissociation processes. His present work is focussed on fundamental aspects of reaction dyanmics and stereodynamics from both the theoretical and experimental points of view.

Luis Bañares received his B.S. degree in Chemistry in 1985 from Universidad Compultense de Madrid, Spain and received his Ph.D. from that same university in 1990. He had postdoctoral stays at the California Institute of Technology (1990−1992) and the Institute of Physics at Wurzburg University, Germany (1995−1996) with Fulbright and Alexander von Humboldt fellowships, respectively. He joined the faculty of the Physical Chemistry Department at Universidad Computense de Madrid in 1992 as an Assistant Professor, becoming a full Professor since 2006. His research interests are related to experimental and theoretical chemical reaction dynamics. His work focuses on the understanding of fundamental chemical reactions and photodissociation processes at a molecular level.

electronic calculations that can cope with the existence of multiple PES correlating with the reagents. Additionally, accurate quantum dynamical calculations become much more demanding since the existence of a deep well in the ground PES implies very many bound states which have to be adequately treated in a rigorous calculation. For these reasons, it was not until the end of the 1990s that these reactions received the deserved attention.

Two issues have been hotly debated for this family of reactions: the possible contribution of more than one electronic PES and, thus, of different mechanisms to the reactivity, and the energy redistribution and lifetimes associated with the various reaction intermediates. In this work, recent progress on these topics and on other dynamical aspects is discussed, using mostly results from quasiclassical trajectory (QCT) calculations as a common thread. Despite its approximate nature and its inherent limitations for the description of purely quantum mechanical effects, like tunneling, zero-point energies, and resonances, the QCT method has a number of advantages for the description and interpretation of features in reaction dynamics. In particular, a unified mechanistic discussion of the systems under consideration, based on classical collision times, is presented in this work. The present study is essentially centered on results reported since the late 1990s. The reader interested in earlier work is referred to the reviews by Casavecchia[10] and Liu[11] and to the introductions of refs 12−15. Throughout the article, the QCT approach, different quantum mechanical (QM) treatments, and experimental data are compared. The work closes with a summary in which interesting points and open questions are underlined.

Victor J. Herrero received his B.S. degree in Chemistry in 1978 from the Universidad Complutense de Madrid, Spain and his Ph.D. from the same university in 1982. He made a postdoctoral stay at the Max Planck Institut für Strömungsforschung, Germany (1985−1987) with an Alexander von Humboldt fellowship. In 1987, he joined the Instituto de Estructura de la Materia (CSIC) Spain, where he is presently a Senior Researcher. His current research interests are the dynamics of reactive and inelastic collisions, the spectroscopy of atmospheric relevant "ices", and the diagnostics and kinetic modelling of cold plasmas.

II. Potential Energy Surfaces

The reactions considered involve open-shell reagents and products implying more than one electronic PES. Over the last years, much work has been devoted by different groups to the construction of accurate theoretical PESs for the reactions considered. The most relevant characteristics of the potential surfaces derived in these works are reviewed in the present section. Unless otherwise stated, the labels corresponding to the irreducible representations of the point symmetry group C_s (i.e., bent) will be adopted.

A. O(^1D) + H_2. The initial 5-fold degeneracy of the ^1D electronic state of oxygen gives rise to five electronic PESs (see ref 16 for detailed schemes), which provide in principle several concurrent adiabatic and nonadiabatic reaction pathways. The ground state electronic potential surface is the singlet $1\,^1A'$. This surface is highly attractive, barrierless for bent configurations, and correlates the ground state reagents and products via the formation of water in its ground $\tilde{X}\,^1A_1$ electronic state. The global reactivity of the system under study is dominated by this PES over the range of collision energies accessed thus far by experiments ($E_c \leq 0.25$ eV). The PES of the first excited state $1\,^1A''$ ($\tilde{A}\,^1B_1$ in C_{2v} symmetry) also correlates adiabatically with ground state reagents and products. In contrast with the ground

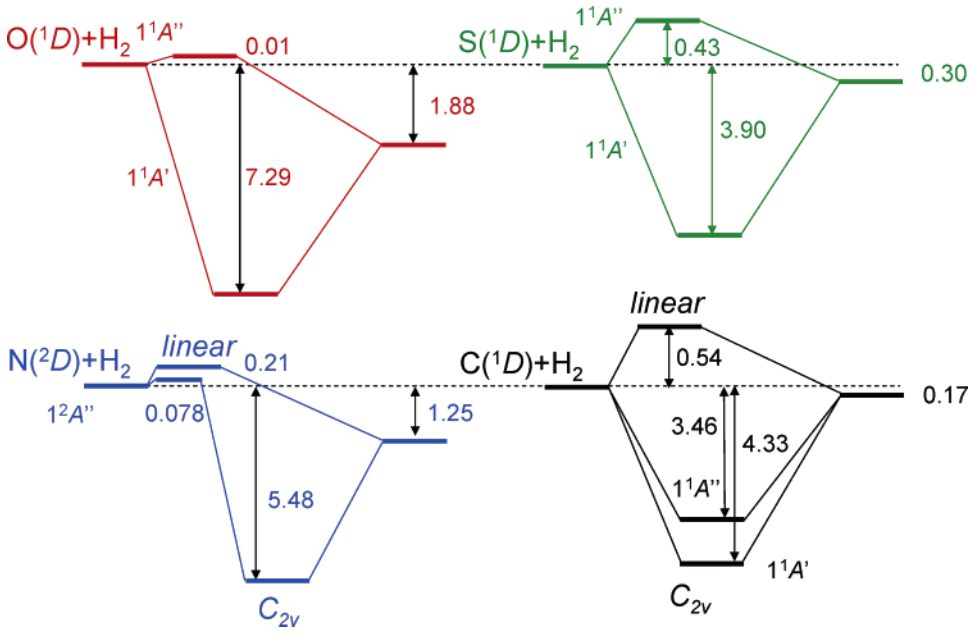

Figure 1. Energy diagrams for the O(^1D) + H_2 (upper left), S(^1D) + H_2 (upper right), N(^2D) + H_2 (lower left), and C(^1D) + H_2 (lower right) systems with indication of the most relevant adiabatic potential energy surfaces involved. Energy values in eV are taken from different references as quoted in Table 1.

state surface, however, it is mostly repulsive with a relatively low (≈0.10 eV) collinear barrier.[17] The next excited surface, $2^1A'$ ($\tilde{B}^1B_1$ in C_{2v} symmetry), has also a similar barrier but correlates with excited-state products, OH($^2\Sigma$)+H($^2S_{1/2}$)). Nevertheless it could contribute to the reaction via nonadiabatic transitions. This PES has an avoided crossing with the $1^1A'$ which gives rise to a conical intersection where the two surfaces are electronically coupled. The other two singlet PESs correlating with ground state reagents, $2^1A''$ and $3^1A'$, ($^1\Delta$ in $C_{\infty v}$ symmetry) are very repulsive in the exit channel, and although they could participate in the reaction via Coriolis coupling with the $1^1A'$, their effective contribution is expected to be negligible.[18,19] The possible crossing between triplet and singlet surfaces in the reactant channel of the O(^3P)/O(^1D) + H_2 system has also been addressed by Schatz and co-workers[20,21] and found to be unimportant even at high collision energies. However, interactions between different surfaces in the exit channel are relevant for the rigorous description of the branching between the multiplet levels in the OH($^2\Pi$) product of the reaction.[22] In summary, the excited electronic states are not expected to play a significant role for collision energies below 0.10 eV, which is roughly the barrier height of the $1^1A''$ and $2^1A'$ PES.

Three-dimensional (3D) calculations of the PESs mentioned in the previous paragraph have been gradually refined. In 1996 Ho et al.[23] constructed a global ground-state PES using a new set of ab initio multireference configuration interaction (MRCI) data and a general multidimensional interpolation based on the reproducing kernel Hilbert space (RKHS) method. Soon thereafter, Schatz et al.[24] reported a calculation of the first excited adiabatic surface using the same methodology. It was found that this excited PES has an early collinear barrier of 0.10 eV which increases quite rapidly for bent configurations. These surfaces are usually referred to as the $1^1A'$ and $1^1A''$ K (sometimes also RKHS) PESs. Trajectory calculations run on them led to a good global agreement with available experimental data, although some discrepancies were also found (see below). By the time of its publication, the $1^1A'$ K surface superseded all of the previous versions of the ground state PES and, in particular, the one of Schinke and Lester,[25] which had been widely used for more than a decade.

TABLE 1: Energetics of the Ground State Potential Energy Surfaces for the O(^1D) + H_2, S(^1D) + H_2, N(^2D) + H_2, and C(^1D) + H_2 Systems with Energy Values in eV

system	exothermicity	C_{2v} min	C_{2v} barrier	linear barrier
O(^1D) + H_2 $1^1A'^a$	1.88	7.29	0.00	0.01
S(^1D) + H_2 $1^1A'^b$	0.30	3.90	0.00	0.00
N(^2D) + H_2 $1^2A''^c$	1.25	5.48	0.078	0.21
C(^1D) + H_2 $1^1A'^d$	0.17	4.33	0.00	0.54

[a] References 26 and 27. [b] Reference 52. [c] Reference 36. [d] Reference 42.

Dobbyn and Knowles[26,27] used the internally contracted MRCI method to compute global potential energy surfaces for the $\tilde{X}$ ($1^1A'$), $\tilde{A}$ ($1^1A''$), and $\tilde{B}$ ($2^1A'$) states of H_2O. Valence correlation effects were well taken into account, and the level of these ab initio calculations was higher than that of the previous PESs. The adiabatic surfaces were transformed to a diabatic Hamiltonian matrix through a diabatization of the $\tilde{X}$ and $\tilde{B}$ states based on their transition angular momentum matrix elements with the $\tilde{A}$ state, and the resulting diabatic functions were then fitted to a 3D analytic form. They are usually known as DK PESs. The main energetic characteristics of the $1\ ^1A'$ and $1\ ^1A''$ DK surfaces are shown in Figure 1 and listed in Table 1. The reaction has an appreciable exothermicity (1.88 eV) and a maximum well depth of 7.29 eV for a C_{2v} geometry measured from the minimum of the asymptotic reactants' valley. The $1^1A'$ DK PES is barrierless for bent configurations and has a very small barrier (0.01 eV) for the collinear approach. The DK PESs are slightly more accurate than the corresponding K surfaces. In particular, the $1^1A''$ DK PES seems to be free of small spurious features in the entrance channel, and it is more reliable in the exit channel, providing a better description of the influence of H_2 rotation on reactivity and of the products rotational distribution.[12,28]

Other potential energy surfaces for this system, based on ab initio calculations and on the double many body expansion (DMBE) procedure have also been reported.[29,30] In particular, that by Brandao and Rio[30] includes a careful modeling of long-range interactions and of the bottom of the H_2O well.

B. N(^2D) + H_2. Five doublet potential energy surfaces correlate to N(^2D) + H_2. The lowest of these surfaces corresponds to the $1^2A''$ ($\tilde{X}^2B_1$) state and should determine essentially the reactivity. In 1999, Pederson et al.[31] reported a global PES for this $1^2A''$ state based on the application of the RRKH space interpolation method to high quality MRCI−SOCI data. The results showed that the surface had a barrier both for collinear and for perpendicular approach, but the latter was much smaller and in fact, the C_{2v} geometry was the only one allowing reaction at thermal energies. A previous, lower order ab initio calculation by Kobayashi et al.[32] had led to a reverse relative height for the $C_{\infty v}$ and C_{2v} barriers, that had to be corrected empirically.[33] QCT calculations on the $1^2A''$ surface of Pederson et al.[31] could reproduce the experimental products' state distribution and differential cross sections.

A PES for the excited $1^2A'$ ($\tilde{A}^2A_1$) state of the system based on a similar methodology was also reported by Pederson et al.[34] This state does not correlate adiabatically to the ground state $^3\Sigma^-$ of NH but to the $\tilde{a}^1\Delta$ excited state, which is endothermic by more than 0.34 eV with respect to the N(^2D) + H_2 asymptote and should thus be of no importance at low collision energies. However, this excited surface interacts with the ground state for linear HNH geometries where the two surfaces form a degenerate ($^2\Pi$) Renner−Teller coupling pair. The barrier for reaction over the excited $1^2A'$ PES is only ≈0.043 eV higher than that of the ground state, and it could contribute to reaction via nonadiabatic transitions. Estimates using a capture model suggest that the contribution should be small at thermal energies.[34,35] Subsequent QCT calculations by Santoro et al.[35] indicate that the reaction on the upper PES leads to an almost exclusive formation of NH($^3\Sigma^-$) at low collision energies but that this contribution is relatively minor.

An improved version of the $1^2A''$ PES of Pederson et al.[31] has been recently presented by Ho et al.[36] The improved surface uses a larger set of ab initio points and a fast algorithm for the computation of the PES and of its gradients, whose fast evaluation is crucial for large scale QCT calculations. The refined surface is free from small spurious features and in better agreement with the ab initio points in some key regions including the collinear and C_{2v} barriers. A summary of the energetics of N(^{2}D) + H_2, based on the PES of Ho et al.[36] is given in Table 1 and Figure 1. Note the comparatively high exothermicity of 1.25 eV, the small insertion barrier of just 0.078 eV and the deep well of 5.48 eV.

More recently, Varandas and Poveda[37] modeled a new DMBE (double many body expansion) $1^2A''$ PES constructed with a larger basis set, although with less ab initio points. The barriers for C_{2v} insertion and for collinear abstraction are about 0.3 kcal mol^{-1} (0.013 eV) higher than in the above-mentioned PES by Ho et al.[36] The cross sections and rate constants calculated on this PES using a wave packet (WP) method and the centrifugal sudden (CS) approximation[38] were found to be in good agreement with the results of ref 36. Finally, it should be mentioned that Qu et al.[39] reported another PES which has been employed to determine cross sections and rate constants for the exchange NH($\tilde{X}^3\Sigma^-$) + D → ND($\tilde{X}^3\Sigma^-$) + H reaction.

C. C(^1D) + H_2. Only two of the five singlet surfaces resulting from the interaction of the fivefold degenerate C(^1D) atom with H_2 correlate with the ground state products: CH($\tilde{X}^2\Pi$) + H(^2S). These surfaces correspond to the singlet ground 1^1A_1 (or $1^1A'$) state and to the excited $^1B_1$ (or $1^1A''$) state. Bussery−Honvault et al.[40] have calculated an ab initio surface for the first singlet state $\tilde{a}^1A_1$ ($1^1A'$) of the CH_2 radical. The authors used multireference single and double configuration interaction (MR−SDCI) calculations with Davidson correction to generate a large set of ab initio data. These points were then fitted to a many body expansion. The resulting PES has a well of 4.33 eV relative to the C(^1D) + H_2 asymptote and is barrierless for perpendicular C_{2v} geometries but has a large barrier (0.54 eV) for collinear approach. The reaction is slightly exoergic by $\Delta H_0^o = -0.27$ eV (−0.17 eV excluding the zero-point energies of the reactants and products; see Figure 1 and Table 1). The surface was employed in QM and QCT dynamical calculations of differential and total cross sections[40,41] which were found to be in good agreement with each other and consistent with available experimental data (see ref 13 and references therein). A further refinement of the PES was achieved through the use of the RKHS interpolation method,[42] which removed spurious features of the original PES and allowed a faster calculation of the surface and its gradients. The efficiency of QCT calculations was largely improved on this refined surface and the results[42] were in very good agreement with those previously obtained on the original PES.[41] More recently, ab initio calculations have also been performed for the $1^1A''$ excited state, and a global PES for this state has been constructed.[43] Interestingly, this PES, which also displays a deep well (3.46 eV relative to the C(^1D) + H_2 asymptote) has high barriers in the entrance channel for $C_{\infty v}$ (≈0.5 eV) and C_{2v} (≈3.6 eV) configurations but presents no barrier for a 60° geometry giving rise to a very interesting dynamics.[44] Intersystem crossing could play, in principle, an important role in this reaction, since the two low-lying singlet and triplet states of CH_2 are known to be strongly mixed. In fact, the interaction of these two states has been invoked to justify the rate constant value calculated for the reverse CH($\tilde{X}^2\Pi$) + H(^2S) reaction.[45] Nevertheless, it was shown that intersystem crossing has no appreciable influence on the direct reaction of H_2 with ground state C(^3P) atoms,[46] and it has not been considered in dynamical studies of the reactive C(^1D) + H_2 system.

D. S(^1D) + H_2. For the S(^1D) + H_2 system, Zyubin et al.[47] carried out extensive MRCI ab initio calculations with multiconfiguration self-consistent field (MCSCF) reference wave functions for the $1^1A'$, $2^1A'$, $3^1A'$, $1^1A''$, and $2^1A''$ surfaces that correlate to the reagents. The collinear barrier for reaction over the $1^1A''$ PES is relatively high (0.43 eV), and consequently, at the moderate collision energies of the available experiments, the reaction must be restricted to the ground state surface. The ground state $1^1A'$ PES was fitted to an analytical function based on the RKHS approach and a Carter−Murrell-type expansion. The surface was checked[48] with QCT calculations and by comparing the results with the experimental data of Liu and co-workers.[49−51] A good global agreement, with some differences in the finer details was obtained. An improved version of the $1^1A'$ PES based on the same ab initio points and using the RKHS interpolation method was produced by Ho et al.[52] QCT results on this improved surface led to a similar level of agreement with experiment. The main energetic characteristics of this reaction are shown in Figure 1 and listed in Table 1. It is slightly exothermic (0.30 eV), and its ground-state PES has a H_2S well depth of 3.90 eV with respect to the separated reagents and is barrierless for all interatomic orientations. In a recent work, Maiti et al.[53] have investigated the role of intersystem crossing in the S(^3P,^1D) + H_2 → SH + H system and found an important interaction in the entrance channel between the first singlet PES, $1^1A'$, and the $1^3A'$ and $1^3A''$ triplet surfaces. The version of Ho et al.[52] was taken for the singlet PES, and the two triplet surfaces were calculated by Maiti et al.[53] at a lower level of theory. Trajectory surface-hopping (TSH)

calculations[53] indicate that intersystem crossing causes a significant electronic quenching of the $S(^1D)$ atoms, leading to a decrease of a factor of 2 or more in the $S(^1D) + H_2$ reactive cross section. This result is however controversial[54] as discussed in the next section.

III. Integral Cross-Sections and Rate Coefficients

Although the reaction probability as a function of collision (or total) energy at a fixed value of the total angular momentum, J, is not a magnitude experimentally accessible, it contains valuable information and constitutes the first step toward the calculation of integral cross-sections and rate constants. Accurate QM calculations by Honvault and Launay[40,41] unveil a rich resonance structure in the energy dependence of the reaction probability for $J = 0$, $P_r(E; J = 0)$, for all of the $A + H_2$ reactions. For the less exoergic $C(^1D) + H_2$ and $S(^1D) + H_2$ reactions, they found very narrow and rapid oscillations, which were much broader and to some extent washed out for the more exoergic $O(^1D) + H_2$ and $N(^2D) + H_2$ systems, where the lowest resonances accessed are more than 1.3 eV above the dissociation limit of the complex formed. Oscillations in the $P_r(E; J = 0)$ are indicative usually of the presence of quantum bottlenecks and/or dynamical resonances. It is expected that long-lived intermediate states give rise to narrow and highly structured oscillations, whereas in shorter lived complexes, the oscillations are broader and weaker. QCT calculations cannot reproduce the resonance structure in $P_r(E; J)$, but retain some of the broader oscillations. However, as it will be shown in section V, the analysis of the reactive collisions shows that reactions exhibiting narrow resonances correlate with much broader distributions of collision times.

By summing over the J converged reaction probabilities, dynamical observables like cross sections or rate constants can be calculated.[41,55−57] It has to be pointed out that QM exact calculations of insertion reactions are considerably more difficult than those of direct abstraction reactions. Symmetric top configurations lie near the potential minimum and are thus energetically accessible. This implies that the Coriolis coupling is significant, and therefore, to calculate the reaction probabilities for this type of reactions, it is necessary to include all possible projections of J onto the body fixed axis, Ω quantum numbers. In addition, due to the presence of a deep well, many rovibrational states have to be taken into account in the close coupling (CC) equations. The centrifugal sudden (also called coupled states, CS) approximation, which neglects the Coriolis coupling between different Ω values at a given J, has been found to perform well in some cases at a less computational cost but in other instances may lead to considerable errors. As expected, the fast resonance oscillations are averaged off and the resulting energy dependence of the cross sections is generally smooth.

In this section, we will concentrate on observables directly comparable to experimental measurements. Most of the available experimental data for cross sections as a function of the collision energy, $\sigma_R(E_{col})$, are restricted to relative values. In this respect, the comparison between accurate experimental values of $k(T)$ and the corresponding theoretical calculations is indeed important to ascertain the participation of electronically excited PESs on the reactivity. Unfortunately, the essentially attractive ground PES, with much smaller barriers, dominates the rate constant values at room temperatures in all cases and the role of excited PESs is only noticeable at $T > 1000$ K.

A. $O(^1D) + H_2$. In the reaction of $O(^1D)$ with the various isotopomers of the hydrogen molecule, the most recent determination of rate coefficients at 298 K by Talukdar and Ravishankara[58] yields values (in $cm^3\ s^{-1}$) of $(1.2 \pm 0.1) \times 10^{-10}$ for H_2; $(1.1 \pm 0.1) \times 10^{-10}$ for D_2; and $(1.2 \pm 0.1) \times 10^{-10}$ for HD. These high $k(T)$ values are characteristic of barrierless reactions. Absolute cross sections for the $O(^1D) + H_2$, D_2, and HD reactions were measured using photolytically produced translationally hot $O(^1D)$ atoms by Koppe et al.[59] and by Laurent et al.[60] at $\langle E_{col} \rangle = 0.12$, 0.18, and 0.14 eV, respectively. From these results, approximate rate coefficients could be derived at high translational temperatures (≈800−1200 K depending on the isotopic variant) but with a room-temperature rotational distribution. The "high-temperature rate coefficients" so obtained are about a factor of 2 larger than those for room temperature,[58] in disagreement with expectations for a reaction without a barrier, whose rate constants should be roughly independent of the temperature.

The evolution of the reaction cross−section with collision energy [i.e., the excitation function, $\sigma_R(E_{col})$], for the $O(^1D) + H_2$, D_2, and HD reactions was measured by Hsu et al.[61] in a crossed molecular beam experiment. Initially, the excitation function (only relative values of $\sigma_R(E_{col})$ were measured) showed a pronounced decline with growing E_{col}, characteristic of a capture reaction without a barrier, but for collision energies higher than ≈0.10 eV, the behavior of the excitation functions deviates from that of a barrierless reaction and they tend to grow with increasing E_{col}. The thermal rate constants can be approximately expressed in terms of the experimental $\sigma_R(E_{col})$.[11,61] The $k(T)$'s thus obtained, increase with temperature for $T >$ 400 K in qualitative agreement with the rate constant data commented on in the previous paragraph. However, the increase in $k(T)$ between 300 and 1000 K derived from the measured excitation functions is appreciably smaller than the factor two corresponding to the values derived from the hot atom studies.[59,60]

Dynamical calculations on the various PESs available can account for many, but not all, of the experimental facts just described. In particular, the room-temperature rate coefficient is determined by the ground state surface and can be well reproduced by QCT and approximate wavepacket QM calculations on the K and DK versions of the $1^1A'$ PES[23,62,63] as well as on that of Brandão and Rio.[30,64] In all cases, the $k(T)$ value for the $O(^1D) + H_2$ reaction at $T = 300$ K is not too far from 1.0×10^{-10} $cm^3\ s^{-1}$ and thus in good agreement with experiment.[58] A somewhat higher rate constant ($\approx 1.6 \times 10^{-10}$ $cm^3\ s^{-1}$) is obtained in QCT calculations[65] performed on the surface of Varandas.[29]

For experiments involving higher collision energies, the influence of excited surfaces can be relevant. Schatz et al.[24] reported QCT calculations of excitation functions and rate constants on both, the $1^1A'$ and $1^1A''$ K PESs. The effect of the $1^1A''$ K PES on the QCT thermal rate constant was found to be appreciable for temperatures higher than 1000 K, but even with this contribution, the calculated high-temperature rate constants were still markedly lower than the rate coefficients derived from the translationally hot atom studies.[59,60] An estimate of the possible contribution of the $2^1A'$ surface to the reactivity did not change this conclusion.[12,24] Reaction cross sections were also calculated on the DK potential surfaces using QCT (see refs 12, 28, and 62). In Figure 2a, the comparison of the $\sigma_R(E_{col})$ obtained by the QCT method and by rigorous QM time independent (TI) approach, based on hyperspherical coordinates,[56] are shown for the $O(^1D) + H_2$ reaction on the $1^1A'$ DK PES, revealing an excellent agreement between the two sets of results. Similar calculations have been carried out by an approximate wave packet QM method[28,62,66] and a quantum

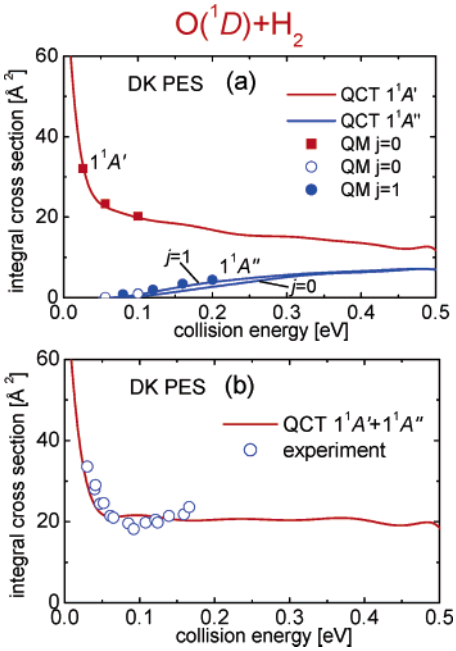

Figure 2. Collision energy dependence of the integral cross section (excitation function) for the $O(^1D) + H_2$. (a) Comparison between exact time−independent (TI) QM and QCT results on the ground $1^1A'$ and first excited $1^1A''$ DK potential energy surfaces for $j = 0$ and $j = 1$ as indicated in the figure. Solid squares: QM calculations on the $1^1A'$ surface from ref 56. Open and solid circles, TI QM calculations on the $1^1A''$ PES, present work. Solid lines: QCT calculations for $j = 0$ on the $1^1A'$ PES for, and for $j = 0$ and $j = 1$ on the $1^1A''$ PES, present work. (b) Comparison of experimental (open circles) and QCT excitation functions at the rotational temperature of the experiments. The QCT excitation function is the sum of the cross sections on the $1^1A'$ and $1^1A''$ PESs. The experimental points have been scaled to the QCT data by a least-square factor.

statistical model (SQM) developed by Manolopoulos and co-workers.[67,68] This model combines a coupled-states capture theory and statistical arguments[67] and simplifies enormously the solution of the problem since no propagation is needed in the PES region corresponding to the collision complex region. The basic assumption of the SQM is that the dynamics of the collision complex is ergodic; this assumption is well justified for a sufficiently deep well and relatively long-lived collision complex. The good agreement between the results of the rigorous calculations and those of the much simpler SQM is certainly encouraging. The cross sections calculated on the $1^1A'$ DK PES were in good agreement with those on the $1^1A'$ K PES and also with the recent approximate (CS) wavepacket calculations of Lin and Guo[64] on the new $1^1A'$ PES of Brandão and Rio.[30]

The shape of the excitation functions for the $O(^1D) + D_2$ reaction and for the OH + D channel of $O(^1D)$ + HD reaction could be well accounted for by these QCT results including both PESs, but the experimental excitation functions[11,61] for the $O(^1D) + H_2$ reaction and for the OD + H product channel of $O(^1D)$ + HD, at collision energies higher than $E_{col} = 0.10$ eV, seem to indicate a rise somewhat more pronounced than that obtained by QCT calculations on the $1^1A' + 1^1A''$ K and DK PESs. The comparison between the QCT cross sections and the experimental excitation function by Hsu et al.[61] (scaled to the theoretical results) are shown in Figure 2b. The QCT data include the contributions of both the ground and first excited PESs. Although the agreement is reasonable, the experimental data seems to indicate a minimum at $E_{col} \approx 0.10$ eV and a subsequent rise more pronounced than that obtained by QCT calculations.

The good agreement found in calculations performed on different versions of the ground electronic state does not extend, however, to the first excited electronic PES, where a different dependence of reactivity on rotational excitation was obtained on the $1^1A''$ DK and $1^1A''$ K surfaces. QCT calculations on the $1^1A''$ K surface predicted an appreciable decrease in the post-threshold cross section upon excitation of the first rotational level of H_2.[24] In contrast, classical, TI and wavepacket QM calculations on the $1^1A''$ DK PES[12,28] led to a higher reaction cross section for $j = 1$ than for $j = 0$, as shown in Figure 2a for the $O(^1D) + H_2$ reaction. This positive effect of the rotational excitation on the reactivity is in qualitative agreement with the experimental results of Lee and Liu,[69] who measured $\sigma(E_{col})$ for the $O(^1D) + H_2$ reaction using either *n*-H_2 or *p*-H_2 and found that at $E_{col} \approx 0.1$ eV, where the $1^1A''$ state is expected to contribute to the overall reactivity, the cross section for $j = 1$ was larger than for $j = 0$. These authors suggested that the observed rise in the excitation function beyond $E_{col} \approx 0.1$ eV was essentially due to reaction of the oxygen atoms with $H_2(j = 1)$ molecules. However, the rise predicted in the theoretical calculations was smaller than the experimental one and, as can be seen in Figure 2a, the difference in the $j = 0/j = 1$ reactivity on the $1^1A''$ PES becomes smaller as E_{col} increases. A close inspection[12] revealed that small, possibly spurious features of the $1^1A''$ K PES give rise to orientational effects, usually associated with negative rotational influence, which are less important or absent in $1^1A''$ DK PES.

A very slight and somewhat unexpected negative effect of rotation at low collision energies, obtained in QCT and approximate QM calculations both on the K and DK $1^1A'$ surfaces,[28,63] was found to be consistent with crossed beam experimental results of Yang and co-workers[28] at $E_{col} = 0.056$ eV and was attributed to the anisotropy of the ground state potential favoring a perpendicular approach over a collinear attack.

B. $N(^2D) + H_2$. As seen in the previous section, the $N(^2D) + H_2$ system is the only one, among those considered in the present work, having a barrier in the entrance channel of the ground $1^1A''$ PES for all interatomic orientations. The rate coefficients measured for this reaction[70,71] are consequently much smaller than the rest. QCT calculations for $N(^2D) + H_2$ on the surface of Pederson et al.[31] gave, as expected, a translational excitation function, $\sigma_R(E_{col})$, with a threshold followed by a rapid rise and a stabilization at higher E_{col}. Later measurements by Liu[11] confirmed the shape of $\sigma_R(E_{col})$ in the post-threshold region.

QCT calculations of k ($T = 300$ K) on this surface and an estimate of $k(T)$ using accurate QM total reaction cross sections led to values of 1.90×10^{-12} and 2.51×10^{-12} cm^3 s^{-1} respectively,[72] suggesting that tunneling may play a role in the reactivity at this temperature. In any case, both the QCT and QM k ($T = 300$ K) values are not too far from the latest experimental datum of $(2.44 \pm 0.34) \times 10^{-12}$ cm^3 s^{-1} [70] or the recommended value of 2.2×10^{-12} cm^3 s^{-1}.[71]

QCT calculations on the improved surface of Ho et al.[36] led to somewhat larger thermal rate constants. At $T = 300$ K, the QCT rate constant for $N(^2D) + H_2$ in the new PES has a value of 2.19×10^{-12} cm^3 s^{-1},[36] even closer to the experimental measurements. The slightly lower barrier of this PES is probably the cause of the higher QCT rate constant. At room temperature, the QCT rate coefficients for reaction with H_2 and D_2 are in good agreement with the experimental ones. Those from the

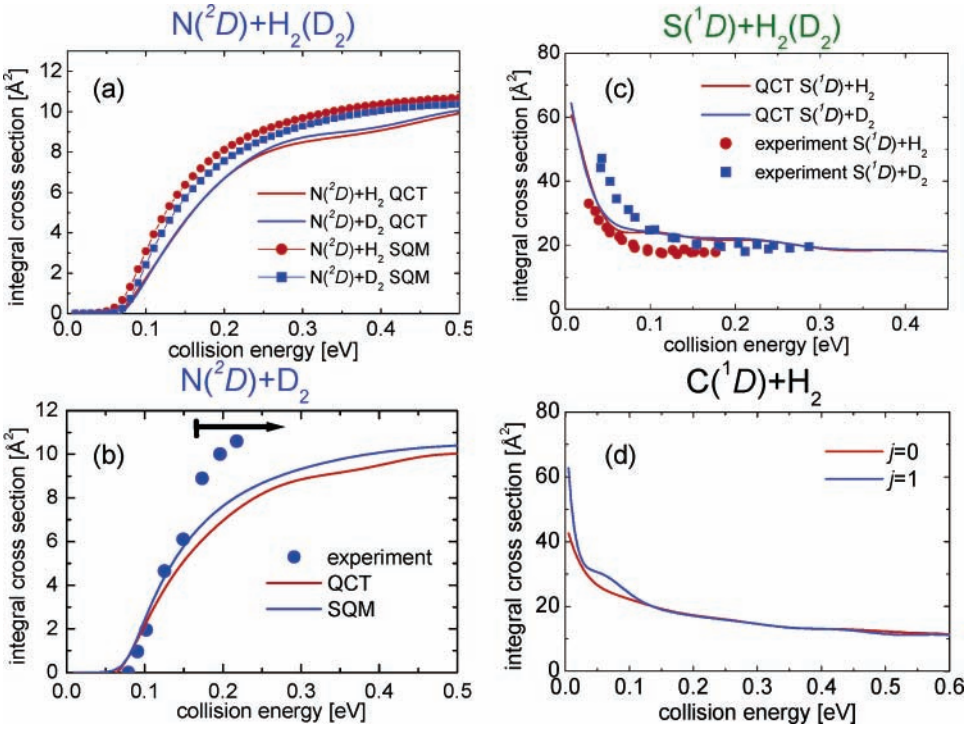

Figure 3. Excitation functions for the $N(^2D) + H_2/D_2$ (a), $N(^2D) + D_2$ (b), $S(^1D) + H_2/D_2$ (c), and $C(^1D) + H_2$ (d) reactions. (a) Solid lines are QCT results and points are SQM results taken from ref 73. (b) Comparison between experimental (solid circles), QCT, and SQM excitation functions for the $N(^2D) + D_2$ reaction. The arrow indicates the range of energies where the $OH + D_2$ reaction can contribute to the total D atom experimental signal (see ref 11). The experimental results have been scaled to the SQM data. (c) Comparison between experimental (circles $S(^1D) + H_2$, squares $S(^1D) + D_2$) and QCT (solid lines) excitation functions. QCT results taken from ref 54. Experimental results from ref 49. Theoretical results from ref 73. (d) Comparison between the QCT excitations functions for $j = 0$, 1 (data from ref 42).

SQM method are somewhat higher, especially for the reaction with H_2. Subsequently, Lin and Guo[74] have used a CC wave packet method to calculate the excitation function in a shorter range of collision energies (up to 0.25 eV) and $j = 0$ and 2. Using these results, the thermal $k(T)$ at $T = 300$ K was estimated to be 2.87×10^{-12} cm^3 s^{-1}, higher than the QCT and experimental results but slightly lower than that obtained by the SQM method.[73] The lower values obtained in the QCT results can be attributed to the lack of tunneling through the barrier, whereas the discrepancies between exact QM and those using the SQM can be possibly due to the fact that this reaction is not completely statistical. The fact that the QM $k(T)$ are higher than the experimental data suggests that the accuracy of the PES close to the barrier needs to be refined and that possibly its height is somewhat underestimated in the PES of Ho et al.[36] In this respect, it is interesting to mention the very recent CS WP calculations by Chu et al.[38] on a new PES[37] considered in section II.B yield a value of the rate constant at 300 K of $\approx 2.0 \times 10^{-12}$ cm^3 s^{-1}. In any case, the results just commented on render very unlikely an appreciable non adiabatic contribution of excited surfaces to the reactivity, as suggested in refs 34 and 35. Recent WP CS calculations by Defazio and Petrongolo,[75] including the couplings between the $1^2A''$ and $1^2A'$ PESs, seem to indicate that, although the contribution from the upper PES is not negligible, some reactivity is also borrowed from the ground PES and the net $k(T)$ is very similar to that obtained within the BO approximation.

QCT excitation functions up to $E_{col} = 0.5$ eV and reagent rotational states $j = 0-4$ and rate constants for the reactions with H_2, D_2, and HD have been compared recently with those obtained with the SQM approach[73] using the PES of ref 36. The results for the $N(^2D) + H_2/D_2$ and initial rotational state $j = 0$ are shown in Figure 3, panels a and b, respectively. The role of molecular rotation in the entrance channel of this reaction has been also addressed in detail in ref 73 using both QCT and SQM calculations. The CS approximation was used for the calculations of integral cross sections in the SQM case. Interesting discrepancies have been found between the classical and SQM results. Whereas a net positive effect of reagent rotation on reactivity is always observed in the classical case, only a very slight influence, restricted to the asymmetric $N(^2D) + HD$ variant, is seen in the SQM calculations. The appreciable classical dependence of $\sigma_R(E_{col})$ on reactivity has to do with the restrictions imposed by the barrier and the orientational properties of the entrance barrier. This behavior is reminiscent of that found for the $F + H_2$ system, which has also a barrier in the entrance channel and a similar kinematics. In the case of $F + H_2$, however, the net effect of rotation was obtained both classically and quantum mechanically (see for instance refs 76 and 77 and references therein). The absence of appreciable rotational effects in the SQM results for $N(^2D) + H_2$ is in this respect puzzling. The most recent QM WP calculations of the $j = 0$ and 2 excitation functions for this reaction[74] seem to give a somewhat positive effect of rotation, although less marked than in the QCT case. Approximate CS WP calculations[38] on the newest PES[37] are not conclusive with respect to the role of initial rotation on the reactivity. Although the calculated specific $k(T; j)$ suggest that the reactivity increases slightly with j, the authors admit that the rotational excitation does not have a significant influence on the reactivity. It is probably worth noticing that the reaction probabilities neglecting Coriolis coupling (CS) reported in that work[38] differ from those using the exact CC. Both the QCT and SQM calculations[73] can account for the post-threshold rise in the $N(^2D) + D_2$ excitation function observed by Liu.[11] The comparison between the experimental (scaled to the theoretical data), QCT, and SQM excitation functions are portrayed in Figure 3 b. The faster rise in the experimental $\sigma_R(E_{col})$ for collision energies higher than

0.2 eV is most probably due to the concurrence of the OH + D_2 reaction in the experimental arrangement.[11]

In summary, although the dynamics of this reaction is overall well accounted for by the most recent PESs (see section IV.B), there persist some interesting discrepancies with the experimental values of the $k(T)$. Of all the insertion reactions here examined the $N(^2D) + H_2$ one is probably the less "statistical" and the one for which the effect of initial rotation might be more significant.

C. $C(^1D) + H_2$. The most recent measurements of thermal rate constants for the reaction of $C(^1D) + H_2$ and its deuterated isotopomers have been published by Sato et al.,[78] who reported values of $(2.0 \pm 0.6) \times 10^{-10}$, $(1.7 \pm 0.4) \times 10^{-10}$, and $(1.4 \pm 0.3) \times 10^{-10}$ cm^3 s^{-1} for H_2, HD, and D_2, respectively. The most recent calculations by Lin and Guo[79,80] using a wavepacket version of the SQM (WP−SQM)[79] on the RKHS $1^1A'$ surface[42] yield values fairly close to the experimental ones at 300 K (1.5×10^{-10}, 1.29×10^{-10}, and 1.13×10^{-10} cm^{-3} s^{-1}). Approximate estimates, based on wavepacket calculations using the reaction probability for $J = 0$ and $v = 0$, $j = 0$ in combination with a capture model, render somewhat lower values.[81] The calculated excitation functions,[79,80] up to $E_{col} = 0.2$ eV, showed an initial sharp decrease at low collision energies followed by a gradual stabilization at higher energies typical of barrierless reactions (see Figure 3d). The comparison between CS and exact CC wavepacket reaction probabilities[82] seems to indicate that the CS approximation underestimates the reactivity considerably. The $\sigma_R(E_{col}; v = 0, j = 0)$ evaluated with this approximation turned out to be noticeably smaller than that obtained with a capture model in conjunction with some CC partial waves and, consequently, the $k(T)$ at $T = 300$ K was smaller by almost a factor of 2. In contrast, there is a very good agreement between the CS and CC capture probabilities calculated with the WP−SQ model,[80] apparently due to the fact that capture dynamics occurs at long range where the Ω can be considered a good quantum number. In addition, the value of the cross section at $E_{col} = 0.08$ eV was in agreement with the exact QM result of ref 41.

QCT calculations of excitation functions for the reactions of $C(^1D)$ with H_2 have also been reported on the same PES[42] (see Figure 3d). Although the qualitative trend is similar to that obtained in the WP−SQM calculations,[79,80] there are some differences in the detailed shape (see Figure 2 of ref 79). The QCT excitation functions are smaller than those from the WP−SQM calculations in the collision energy range for which the statistical QM model calculations are available (0−0.2 eV), especially at the lowest E_{col}. The excitation functions for the three H_2 isotopomers are very similar with some differences at energies below 0.02 eV. It should be noticed that the calculation of rate constants at temperatures below 200 K poses a serious problem for QCT and TD-QM methods when there is no reaction threshold. At low collision energies, propagation times and initial distances need to be increasingly large, making the calculations computationally more demanding and subject to larger errors. Experimental measurements of the evolution of the integral cross sections of $C(^1D) + D_2$ with collision energy reported by Liu[11] confirm the behavior observed in the theoretical calculations.

The final remark in this subsection is about the contribution of the $1^1A''$ PES to the overall reactivity. The QM and QCT results obtained in ref 44 indicate that the cross section at $E_{col} = 0.08$ eV on the $1^1A''$ PES is about one-half of the value on the $1^1A'$ PES. However, up to date no excitation functions have been calculated for an extended range of energies. Assuming that the reaction on this excited PES has no threshold, the contribution of the $1^1A''$ PES might be roughly estimated as ≈50% of that obtained on the ground singlet PES. Still the values of the theoretical $k(T)$ would be compatible with the experimental results within their error limits. A definitive assessment of this contribution and hence of the PES is clearly required.

D. $S(^1D) + H_2$. Excitation functions for the $S(^1D) + H_2$, D_2, and HD reactions have been obtained by different groups. Chao and Skodje[48] reported QCT calculations on the surface of Zyubin et al.[47] The results showed once more the typical barrierless behavior: a marked decrease in the cross section at lower energy, followed by a stabilization as the collision energy increases in good agreement with the measurements of Lee and Liu.[49] Later QCT calculations on the globally smooth surface of Ho et al.[52] led to similar results. Further QCT work[54] performed on the latter PES showed that rotational excitation of the H_2 molecule up to $j = 3$ has no effect on the reaction cross sections. In the same work, Bañares et al.[54] derived the excitation functions using accurate time independent QM reaction probabilities for $J = 0$ and a capture model.[28,62] These $\sigma_R(E_{col})$ were slightly smaller than the classical ones, but both the QCT and capture model results could reproduce the shape of the experimental excitation functions. The comparison is shown in Figure 3c. A similar agreement was obtained by Lin and Guo[83] on the same PES using WP−SQM with the CS approximation. However, the cross sections obtained in the latter work were somewhat larger than those reported by Bañares et al. All of these theoretical QCT and approximate QM calculations led to almost identical excitation functions for the three isotopic variants (summing the SH + D and SD + H channels for the reaction with HD) in contrast with the experimental data,[49] as shown in Figure 3c.

Room-temperature rate constants for $S(^1D) + H_2$ derived from the excitation functions of Bañares et al.[54] and of Lin and Guo[83] are in the $1.3-1.5 \times 10^{-10}$ cm^3 s^{-1} range and thus somewhat lower than the experimental value[84] k ($T = 300$ K) $= 2.1 \times 10^{-10}$ cm^3 s^{-1}. Lin and Guo argued that the experimental rate constant may be overestimated and contain some contribution from nonreactive pathways. For the derivation of the theoretical rate coefficients, the value directly obtained from the convolution of the excitation function has been multiplied by the usual multisurface factor of (1/5), which accounts for the 5-fold degeneracy of the reagent's channel. As indicated above, Maiti et al.[53] have suggested in a recent work that electronic quenching due to intersystem crossing might reduce the cross section on the ground state surface by a factor of 2. However, this reduction would have a noticeable effect on the calculated rate constants and would lead to a worse agreement with experiment.

The intramolecular kinetic isotope effect, k_{DS+H}/k_{HS+D}, predicted in ref 54 is 1.08 and compares very well with the experimental results of ≈1.0 by Inagaki et al.[85] The result obtained by Lin and Guo using the WP−SQM is considerably higher, ca. 2.1.[83]

IV. Products' State Distributions and Differential Cross-Sections

Measurements resolved in the scattering angle and the internal states of the products provide in principle a more sensitive test of the dynamics. For the present family of reactions they could be very advantageous in order to clarify the contribution of different potential surfaces to a given reaction, since the microscopic mechanisms are usually very different for the

ground and excited PES. The exact QM calculation of the differential cross sections (DCS) and internal state distributions is also much more demanding than that of total cross sections or rate constants, since it is necessary to account for all partial waves and the Coriolis coupling of all of the projections Ω of J onto the body fixed axis. In general, these calculations are restricted to relatively low E_{col} and to the H_2 isotopomer. In the case of time dependent QM methods, the difficulties arise from the necessary projection of the wave packet on the final state which requires a finer grid. The situation gets even more complicated if nonadiabatic effects are to be considered. Fortunately, QCT and SQM results are in most cases in good agreement with the exact QM results and account very well for the experimental available results. Unless otherwise stated, the angular distributions in this section are always referred to the center-of-mass (CM) frame.

A. O(^1D) + H_2. The O(^1D) + H_2 system and its isotopic variants have been studied with special detail and have benefited from great improvements in the experimental techniques during the past decade. It is instructive to review briefly the recent experimental progress and its fruitful interplay with theoretical advances.

DCS and internal states' populations of the reaction products have been measured since the 1980s.[5,86,87] The QCT calculations of Schatz et al.[24] on the $1^1A'$ K PES could account for these early results showing broad internal state distributions, which were nearly statistical subject to the constraints of angular momentum conservation, and for the approximately symmetric backward−forward angular distributions. However, calculations on various versions of the ground $1^1A'$ PES have shown that state resolved DCS can be strongly asymmetric with clear predominance of scattering into the forward or backward hemispheres.[88,89] During the 1990s, a series of new molecular beam experiments by Liu and co-workers[90−93] and by Casavecchia and co-workers[94,95] led in some cases to asymmetric angular distributions of the OH reaction products, especially for the higher collision energies. The group of Liu used Doppler-selected time-of-flight methods detecting the H or D atoms by (1 + 1) REMPI, and that of Casavecchia employed a refined version of the crossed molecular beam apparatus of Buss et al.[5] Other measurements, based on an imaging technique, were reported by Suits and co-workers.[96] The QCT calculations of Schatz et al.[24] showed that, above the threshold for reaction on the $1^1A''$ PES ($\approx$0.10 eV), the inclusion of the $1^1A''$ PES, giving preferentially backward scattering, induced an asymmetry in the total DCS that led to a somewhat better agreement with the experimental data at higher collision energies.[90] As expected from the topology of the $1^1A''$ PES, its dynamics corresponds to a direct reaction with an early barrier and collinearly constrained, in strong contrast with that on the $1^1A'$ PES. The vibrational distribution is strongly inverted, favoring the population of $v' \geq 3$, and its DCS is strongly backward.[12,24,97,98]

The asymmetric O(^1D) + HD reaction provided a rich dynamical information. Hsu and Liu[91,92] improved the previous experiment of Che and Liu[90] for this same system, and Aoiz et al.[12,97] performed further QCT calculations using both the K and DK PESs. The contribution of the $2^1A'$ DK PES was considered by using a trajectory surface hopping methodology. The calculated angular distributions showed a global good agreement with some differences with respect to those deduced from the experiment.[92] One of the main differences found was the ratio of the backward(180°)/forward(0°) peaks to the sideways(90°) scattering, which was appreciably larger in the experiment than in the calculations.

The primary data in the experiments of Liu and co-workers were angle-resolved translational energy distributions of the products, showing a weak peak structure. The QCT calculations at 89 and 196 meV collision energy by Aoiz et al.[12] could reproduce these peak structures and assign the various peaks to groups of rotational levels coming from different vibrational states. The calculations on the $1^1A''$ K PES led to bimodal rotational state distributions, which was proved to be caused by an artifact in the product channel of that surface. No bimodal distributions were found in the DK $1^1A''$ results, which were in turn in better agreement with experiment.[12]

A further theoretical study the O(^1D) + HD reaction on the $1^1A'$ and $1^1A''$ DK surfaces[98] showed that the abstraction and insertion pathways had very different stereodynamical properties. More specifically, the rotational angular momentum of the OH and OD products is strongly polarized (aligned and oriented) when the reaction takes place on the $1^1A''$, whereas the spatial distribution of $\mathbf{j}'$ is almost isotropic on the ground $1^1A'$ PES. In this study, a detailed comparison of exact QM and QCT vibrationally state resolved distribution of rotational states and DCS, as well as of the polarization moments, was also presented for the two channels of this reaction on the excited PES. The agreement between QM and QCT results was fairly good, with some differences in the absolute values of the cross sections for OH formation. From this study, it become apparent that, in order to fully appreciate the contribution of the excited PES, state resolved measurements of vibrationally excited products were required and that the measurement of vector properties, as the polarization of the angular momentum, would be a very stringent test of the theoretical calculations.

Shortly thereafter, a combined theoretical and experimental investigation exploiting the stereodynamic characteristics of the O(^1D) + H_2 reaction was reported by Aoiz et al.[99] The measurements were carried out by Brouard and co-workers using velocity aligned O(^1D) atoms generated by photolysis and taking advantage of the orientational properties associated with the use of polarized laser light (see refs 88 and 100 and references therein). These experiments have a low angular and, depending on the precursor, low energy resolution, but they are specific for a single rovibrational state of the products and allow a precise determination of the rotational populations by laser induced fluorescence. The theoretical study included QCT and exact QM results on both the $1^1A'$ and $1^1A''$ DK surfaces. The accurate QM calculations on the $1^1A'$ PES were performed with the hyperspherical coordinate methodology of Launay and co-workers already mentioned in the previous section. For the conditions of the experiment (average collision energy 120 meV with a full-width at half-maximum, fwhm, of 160 meV), a significant fraction of the collisions take place at energies higher than the threshold for reaction on the $1^1A''$ PES. A noticeable contribution of the abstraction mechanism to the production of the highest vibrational states ($v' = 3$ and 4) of the OH was evinced in this study, and it was clearly shown that the experimental rotational distribution for $v' = 4$ could only be accounted for if the participations of the two PESs were taken into account. In addition, a careful determination of the $a_0^{\{2\}}$ alignment moment (alignment of $\mathbf{j}'$ along the initial relative velocity) for several rotational states of the $v' = 4$ manifold was carried out and found to be in quantitative agreement with the QM and QCT calculations when both the $1^1A'$ and $1^1A''$ PESs were considered. Hence, the theoretical predictions which indicate a strong contrast in the degree of polarization of the final rotational angular momentum, $\mathbf{j}'$, with respect to the initial relative velocity vector, $\mathbf{k}$, on both PESs, were confirmed.[99]

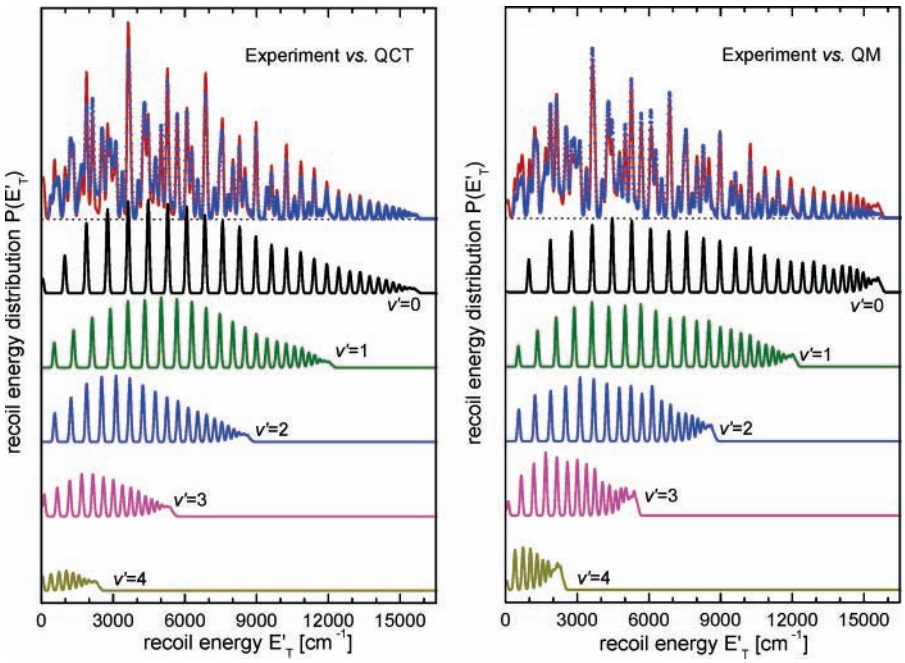

Figure 4. Experimental (red) product recoil energy distribution for the $O(^1D) + H_2(v = 0, j = 0)$ reaction at 56 meV collision energy compared to simulations (blue) carried out with (left) the QCT and (right) the QM state-resolved integral cross sections. Each of these two theoretical distributions is independently scaled to the experimental data with a single least-squared factor. The theoretical v' state-resolved recoil distributions are also shown in the lower part of the figures to guide the assignment of the experimental spectrum. Adapted with permission from Figure 9 of ref 105. Copyright 2002, American Physical Society.

Overall, the importance of this study lies in the fact that for the first time the participation of the excited PES could be quantitatively assessed.

A large increase in experimental resolution was achieved by the group of Yang[28,101−106] by applying the Rydberg-tagging technique,[107,108] based on the promotion of the product H atoms to a Rydberg state and their subsequent field ionization. The highest energy resolution achieved thus far corresponds to the $O(^1D) + H_2$ isotopic variant at a collision energy of 56 meV,[102,105] where the rovibrational distribution of the scattered OH molecules could be measured at a number of laboratory angles. A first analysis of these results[102] led to the somewhat unexpected conclusion that a small contribution of the collinear abstraction mechanism over the $1^1A''$ PES could be identified even at this low collision energy. However, a rigorous theoretical simulation based on thorough QCT and accurate QM results demonstrated the contrary.[105] The good agreement between the measured and simulated recoil angular distributions of the H atoms is exemplified in Figure 4, which shows also the concordance between the two theoretical approaches. The high experimental resolution allowed even the separation of the two spin−orbit components in $v' = 4$, whose populations were found to be statistical.[105] A comparison between the theoretical DCSs and that deduced from experiment is also shown in Figure 5. Although the overall agreement is good, there are some differences worth noting, especially the high forward peak in the QM calculation which has no experimental or classical counterpart. A narrow QM peak is also observed in the backward direction. Sharp peaks in the DCS have been associated with tunneling (see also comments in refs 72 and 109) and in favor of this interpretation would be the fact that they were also obtained in the SQM of Manolopoulos and coworkers,[68] which due to the approximations inherent to the model could not reproduce the slight forward−backward asymmetry obtained in the accurate calculations of Honvault and Launay.[56] Since this model makes use of the random phase approximation,[68] interferences between different partial waves

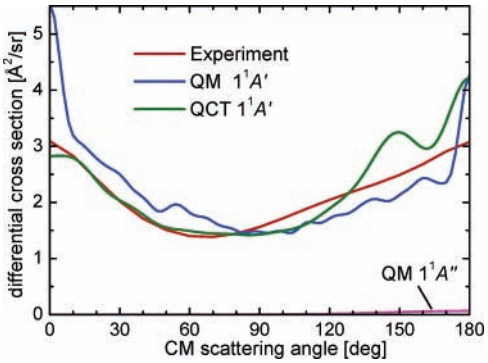

Figure 5. Experimental total reactive differential cross section for the $O(^1D) + H_2(v = 0, j = 0)$ reaction at 56 meV collision energy compared to the QM and QCT calculations on the $1^1A'$ and $1^1A''$ DK PESs. The experimental DCS have been scaled to the QM data. Adapted with permission from Figure 10 of ref 105. Copyright 2002, American Physical Society.

and possible resonances are ruled out as the origin of these sharp backward and forward peaks. However, very recently, Bonnet et al.[110] have questioned that explanation. By comparing the classical results using a phase space model and those obtained with the SQM model,[68] they concluded that the absence of sharp peaks in QCT or classical calculations are due to the fact that the parity conservation is ignored in classical mechanics. These authors have proposed a simple, approximate recipe to incorporate the parity conservation in classical calculations, although its rigorous implementation in QCT calculations is not obvious. The absence of sharp peaks in the experimental results could be due, at least in part, to a certain angular smearing of the measured data.

Very recently, these measurements have been extended to the OH channel of the $O(^1D) + HD$ reaction at $E_{col} = 74$ meV.[106] Angular distributions and kinetic energy spectra were measured and after transformation to the CM frame, and these results were compared with accurate TD QM calculations on

the ground $1^1A'$ DK PES.[106] The agreement between experimental and theoretical calculations is similar to that obtained for the reaction with H_2 at 56 meV. In particular, the experimental total DCS is in excellent accordance with the calculated one, except for the sharp peaks in the extreme forward and backward region, which do not have a counterpart in the experimental results. Interestingly, the QCT DCS, calculated on the same PES at a slightly higher energy, 89 meV,[12] is in even better agreement with the experimental result, as it lacks of the sharp forward/backward peaks found in the QM calculations.

The asymmetry induced in the DCS by the growing importance of the abstraction mechanism with increasing E_{col} is better seen in the $O(^1D) + D_2$ isotopomer. For this isotopic variant of the reaction, the larger mass of deuterium allows to attain higher collision energies experimentally. However, it is interesting to observe that the QCT calculations predict also an increase of the asymmetry with E_{col} for the insertion on the attractive $1^1A'$ PES.[109,111]

In a recent work, Alexander et al.[22] have applied the SQM of Manolopoulos and co-workers to the calculation of product multiplet branching in the $O(^1D) + H_2$ reaction considering the four electronic surfaces ($^{1,3}A'$ and $^{1,3}A''$) that correlate with the products, and have found that although the two spin−orbit manifolds are equally populated, the bond breaking in the H_2O intermediate leads to a strong propensity for the formation of the Π (A') Λ doublet states of OH, which is preserved through the curve crossings of the exit channel. This result is consistent with the available laser experiments directly probing these states.[87,99,112]

B. $N(^2D) + H_2$. Since the mid 1990s, Umemoto and co-workers[113−116] measured ro-vibrational state distributions of the nascent products in the $N(^2D)+H_2$ reaction and its deuterated isotopomers. Noninverted vibrational populations and broad rotational distributions peaking at high j' values, typical of reactions with an intermediate potential well, were found in these experiments. From the absence of leaving-atom isotope effect in the rotational distributions of the NH and ND molecules produced in the $N(^2D) + HD$ reaction, Umemoto[115] concluded that the rotational populations are set by a transition state lying in the exit channel.

For $N(^2D) + D_2$, Casavecchia and co-workers[14,117] carried out crossed molecular beam experiments at collision energies of 165 and 220 meV. The DCS derived from the measurements were approximately backward−forward symmetric and only 30% of the available energy was found to go into products' translation.

QCT,[14,31,36,72,117,118] as well as exact[55,72,118] and approximate[67,68,118] QM calculations of DCS and products' state distributions have been performed on the newest ab initio ground state ($1^2A''$) PESs for this system.[31,36] The collision energy of most calculations is that of the molecular beam experiments, and although it is higher than that of the measurements of Umemoto and co-workers, it is much smaller than the reaction exoergicity, which makes a comparison meaningful. The accordance between experiment and theory is good in the vibrational distributions and less so in the rotational ones. The theoretical results predict hot rotational populations peaking at high j', in rough agreement with those from Umemoto and co-workers; however, the experimental rotational distributions have an appreciably higher population at low rotational levels.[114,115] The global picture of the distribution of internal states corresponds to a statistical behavior compatible with the conservation of energy and angular momentum. Consequently, the exact

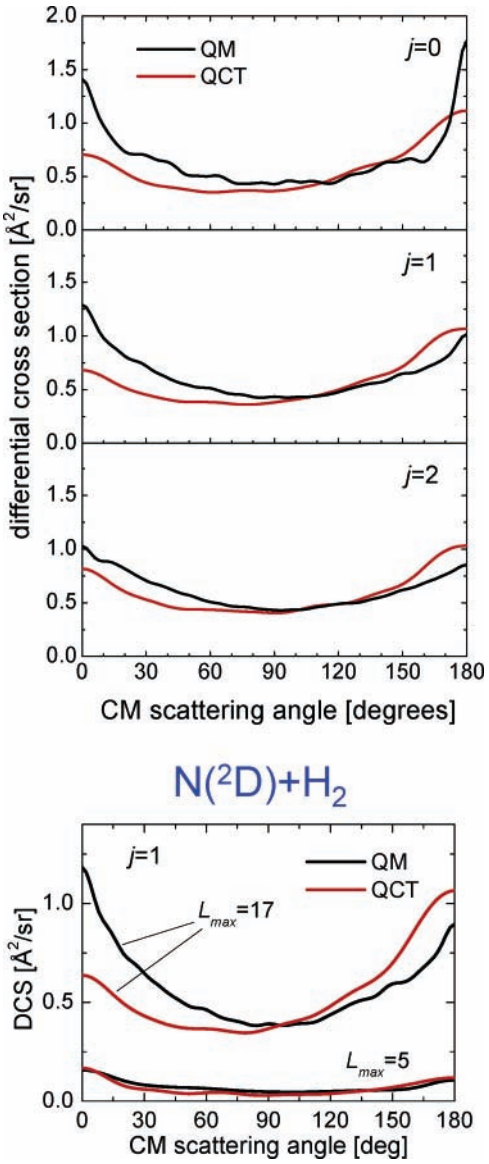

Figure 6. Upper panels: QM and QCT total differential cross sections for different values of initial j of H_2 of the $N(^2D) + H_2$ reaction at 0.165 eV collision energy. Lower panel: Total differential cross section as a function of the maximum orbital angular momentum L_{max} retained in the partial wave sum for the $N(^2D) + H_2(v = 0, j = 1)$ reaction at 0.165 eV collision energy. Adapted with permission from Figures. 2 and 3 of ref 72. Copyright 2002, American Physical Society.

results are well accounted for by the SQM of Manolopoulos and co-workers.[67,118]

Broad angular distributions with backward and forward maxima, consistent with the measured ones within the experimental uncertainty, were obtained in the theoretical calculations. Accurate QM DCSs were found to be slightly biased toward backward or forward scattering depending on the initial j and E_{col}.[55,118] The DCS from the SQM[68,118] are in fairly good agreement with those from exact QM calculations, except for the fact that they are entirely symmetric due to the inherent characteristics of the model. Both types of quantum mechanical calculations showed sharp maxima at 0° and 180°. The corresponding QCT calculations have broader maxima and seem to lack part of the forward hemisphere scattering,[14,31,36,117,118] as can be seen in Figure 6. This contrasting behavior between QM and QCT is analogous to that discussed in subsection IV.A. The issue was addressed in a combined theoretical and experimental study on the $N(^2D) + H_2$ isotopic variant,[72] the

only one for which accurate QM calculations were feasible at that moment. A comparative study of the QCT and QM reaction probabilities and DCSs as a function of the orbital angular momentum, L, indicates that in the QM case larger values of L participate in the reaction.[118] This fact strongly suggests that the discrepancies between the two theoretical approaches in the forward scattering region are due to QM tunneling through the centrifugal barrier (see Figure 6). As mentioned in subsection IV.A, the recent study by Bonnet et al.[110] casts some doubts on this explanation. As initial j increases, the forward and backward peaks tend to smooth out rapidly and the agreement with the QCT results improves.

C. C(^1D) + H_2. Internal state distributions of the CH molecules formed in the C(^1D) + H_2 reaction were measured in the 1980s and 1990s with laser techniques.[119,120] The distributions of rotational levels were found to be nearly Boltzmann-like up to the thermochemical limit. The analysis of the angular and time-of-flight distributions from recent crossed beam experiments[13,121,122] on C(^1D) + H_2/D_2 led to backward−forward symmetric DCS and showed that about 60−70% of the available energy appeared as products translation. Since the reaction is nearly thermoneutral, only $v' = 0$, or at most $v' = 1$, are accessible to the products in the mentioned experiments.

In general, the theoretical calculations on the most recent versions of the $1^1A'$ potential surfaces[40,42] show good agreement with the experimental data. Both QCT[42,121] and QM calculations[41,68,121,122] lead to the backward−forward symmetric DCSs expected for complex-forming insertion mechanisms.[64,121] In general terms, the agreement between exact QM, SQM, and QCT rotational distributions and DCS is somewhat better than for the reactions with O(^1D) and N(^2D). As in other reactions of this family, both types of QM results lead to sharper backward and forward peaks for initial $j = 0$, which were tentatively attributed to tunneling (see, however, ref 110). The theoretically predicted DCSs are in good agreement with the experimental findings although the sharp QM peaks at the extremes of the angular distribution have not been resolved in the measurements. A comparison based exclusively on calculations performed on the $1^1A'$ PES shows some discrepancies in the fraction of energy appearing as products' translation and in the vibrational population of the products. It has been speculated that they may be due to deficiencies in the long-range part of the potential surface, or to the contribution of the excited $1^1A''$ PES.[121,122]

As mentioned in section II.C, very recent QCT and accurate QM calculations clearly show that the $1^1A''$ PES may play an important role and that its contribution to the overall reactivity cannot be neglected.[44] Thus far, calculations are restricted to the reaction with the H_2 isotopomer at $E_{col} = 0.08$ eV and indicate that the dynamics on this excited PES is very different from that on the ground potential. The reaction is much more direct, and if any collision complex were formed, its lifetime would have to be 1 order of magnitude shorter than on the ground PES[44] in spite of the existence of a very deep well.[43] As mentioned in section III.C, the total $\sigma_R(E_{col})$ is ≈50% of that on the 1 $^1A'$ PES and the rotational distribution is broad but nonstatistical. The DCS on this excited PES is fairly isotropic, but it features a strong forward peak in both QM and QCT results. Interestingly, the QCT forward peak is somewhat sharper. Summing the contributions of both PES, the resulting DCS at $E_{col} = 0.08$ eV is slightly asymmetric favoring forward scattering. In addition, the strong polarization of the DCS (ratio between scattering at 0° or 180° and 90°) becomes also smaller, at least with regard to backscattering. Another interesting difference with the dynamics on the ground PES results from the correlation between forward scattering and the highest orbital angular momenta leading to reaction. Although for the whole series of reactions on their ground states this correlation is not clear in either QM or QCT calculations, in the reaction on the excited $1^1A''$ PES, the highest range of L contribute most to the appearance of forward scattering.

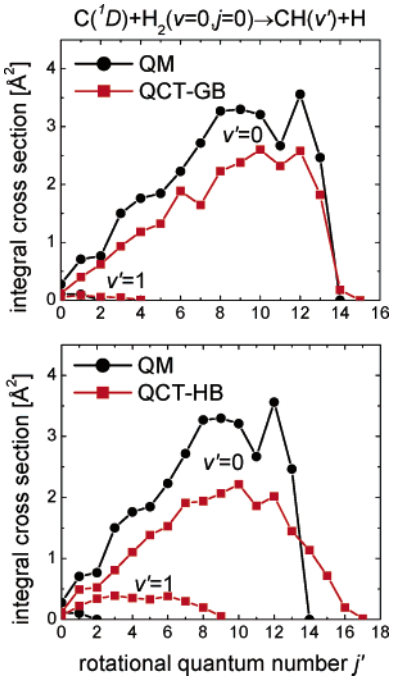

Figure 7. QM and QCT rotational state distributions for $v' = 0,1$ calculated for the C(^1D) + H_2($v = 0, j = 0$) reaction at 80 meV collision energy. Top panel: QCT results obtained by using the Gaussian-weighted binning method to assign product quantum states. Lower panel: QCT results obtained by using the common histogramatic binning method to assign product quantum states. Reprinted with permission from Figure 2 of ref 41. Copyright 2003, American Physical Society.

One of the major shortcomings of the QCT approach is the binning procedure, used to assign the final quantum states. The usual histogramatic method, which consists in rounding the final v' and j' classical values to the nearest integer, can lead to appreciable distortions, especially in the case of slightly endoergic or nearly thermoneutral channels and when the level spacings are large (see, for instance comments on reactions involving muonium in ref 123). As a result of this binning, states not allowed by energy conservation may appear as artificially populated in QCT calculations. This problem can be partly circumvented by the use of a Gaussian-weighted binning procedure based on a method originally proposed by Bonnet and Rayez.[124] The basic idea is the use of a Gaussian function, centered at the right QM values of the vibrational or rotational action, to weight the trajectories. The closer the value of the classical action to the nearest integer, the more weight is given to the corresponding trajectory. The significant improvement achieved with this procedure is shown in Figure 7, where QCT and accurate QM products' distributions are compared.

It is worth noting that the theoretical DCS obtained for the C(^1D) + H_2 system on the $1^1A'$ ground PES exhibits a nearly perfect backward−forward symmetry, whereas those for the O(^1D) + H_2 and N(^2D) + H_2 reactions present certain degree of asymmetry (in the case of O(^1D) + H_2 this is true also for collision energies below 0.1 eV, before the onset of the abstraction mechanism). This more statistical behavior of the HCH reaction complex leads to an excellent agreement between

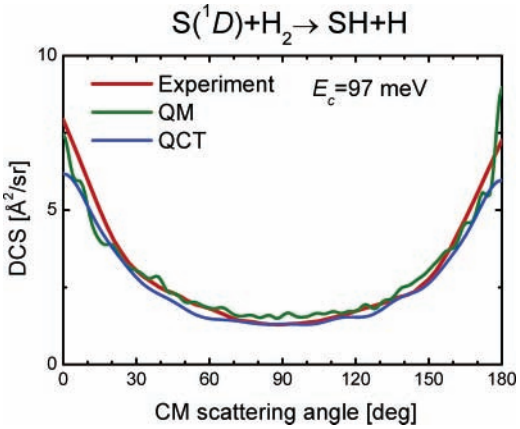

Figure 8. Comparison between experimental and theoretical (QCT and QM) total differential cross section for the $S(^1D) + H_2$ reaction at 97 meV collision energy. Adapted with permission from Figure 8 of ref 126. Copyright 2004, American Chemical Society.

the accurate QM results[41] and those from the SQM model of Manolopoulos and co-workers.[68,122]

D. $S(^1D) + H_2$. In an early experiment, Inagaki et al.[85] obtained information on the translational energy release and isotopic branching ratio for the $S(^1D) + HD$ reaction. Differential cross sections and translational energy distributions of the products for $S(^1D) + H_2$ and $S(^1D) + D_2$ reactions were later reported by Lee and Liu[50,51] in a series of crossed beam experiments using the Doppler-selected REMPI time-of-flight method for the detection of the H and D atoms. A marked backward−forward symmetry was observed in the experimentally deduced DCS. The energetics of the reaction allowed for a significant population of the $v' = 1$ level of the products at the collision energies of the experiments, which could be identified in the structure of the translational energy distributions.

QCT calculations by Chao and Skodje[48] for all the isotopomers of the system carried out on the ab initio surface of Zyubin et al.[47] could account for the most important features of the experiments of Liu and co-workers but led to some differences in the more finely resolved quantities.

Further theoretical calculations[57,68,83,126] were also carried out on the refined surface of Ho et al.[52] In particular, a combined QCT and QM calculation for the $S(^1D) + H_2$ was reported by Bañares et al.[126] The QCT calculations were performed at the two collision energies (0.097 and 0.17 eV) of the experiment of Lee and Liu,[51] but the accurate QM ones were restricted to the lower energy. At 0.097 eV, the agreement between the experimental DCS and those from the two theoretical approaches is virtually quantitative as shown in Figure 8. It is also remarkable the excellent agreement between QM and QCT total DCS and J −partial cross sections (see Figure 16 of ref 126). For $j = 0$, the QM calculations predict a sharp peak confined to the backward direction which disappears for initial $j = 1$; by averaging over initial rotational states the QM sharp peak at 180° is washed out. A similar agreement is obtained (not shown in Figure 8 for clarity) with the results of the statistical QM method,[68] as expected for this very symmetric DCS. At 0.17 eV the experimental DCS is more asymmetric and the agreement between QCT and experiment deteriorates something.[126] The calculations can also reproduce well the shape of the experimental energy distribution, although the classical and quantal results predict a somewhat different contribution from the $v' = 1$ state (see Figure 9). Lin and Guo[83] have performed QM calculations for all the isotopic variants and experimental

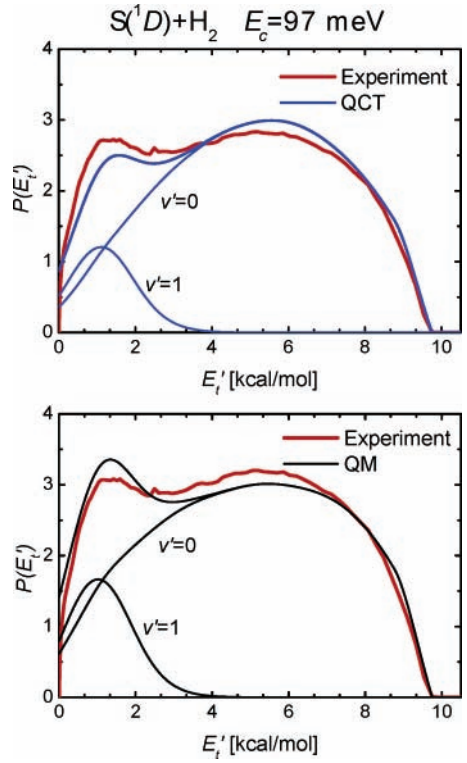

Figure 9. Comparison between experimental and theoretical total and vibrational state-resolved product translational energy distributions for the $S(^1D) + H_2$ reaction at 97 meV collision energy. Top panel: experiment vs QCT. Bottom panel: experiment vs QM. Adapted with permission from Figure 9 of ref 126. Copyright 2004, American Chemical Society.

collision energies using a statistical QM model analogous to that Manolopoulos and co-workers. The calculated DCSs remain essentially symmetric in all cases, whereas some of the measured ones show some asymmetry.

In a recent work, Khachatrian and Dagdigian[15] have investigated the fine structure in the internal state distribution of the SD product from the $S(^1D) + D_2$ reaction. Using LIF, these authors measured a partial rotational distribution for the $v' = 0$ level of SD, which was found to be approximately statistical with a small preference for the formation of the $\Pi_{3/2}$ spin−orbit manifold. In contrast to the analogous reaction with $O(^1D)$ (see above) the populations of the Λ doublet levels A' and A'' of the SD $^2\Pi$ state were found to be roughly equal. In order to clarify this different behavior, multistate statistical QM calculations of the type reported in ref 22 could be very helpful.

V. Collision Times and Reaction Intermediates

As shown in the previous section, approximately symmetrical DCSs and roughly Boltzmann distributions of internal states were mostly obtained for the reactions considered over their respective ground state PESs, but some asymmetry in the DCSs and deviations from statistical distributions were also observed, especially in the $O(^1D) + H_2$ and $N(^1D) + H_2$ reactions. These results point to distinct characteristics of the respective reaction intermediates. Another clue proceeds from the reaction probabilities as a function of E_{col} at a given J. As commented on above, the exact QM $P_r(E;J)$ for the $C(^1D)$ and $S(^1D)$ reactions with H_2 on the ground PES display much more rapid oscillations than the relatively smooth ones obtained for the reactions with $O(^1D)$ and $N(^2D)$.

The analysis of classical trajectories in terms of collision times can provide a valuable information on the nature of the collision

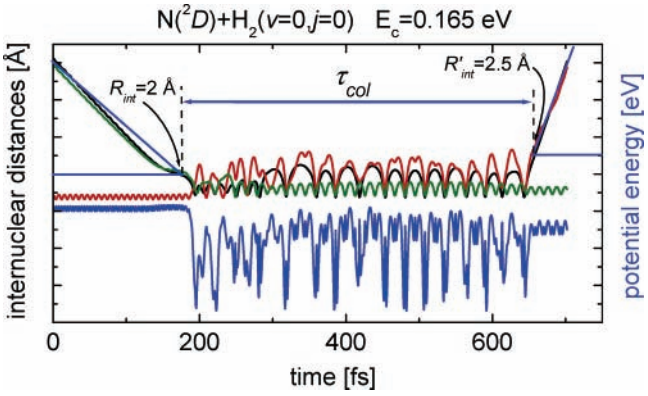

Figure 10. Internuclear distances (black, read and green) and potential energy (blue) as a function of time for a selected long-lived trajectory for the $N(^2D) + H_2(v = 0, j = 0)$ reaction calculated at 0.165 eV. The collision time, τ_{col}, is defines by the two vertical lines in which both the initial (R_{N-HH}) and final (R_{NH-H}) center of mass distances are 2 Å and 2.5 Å, respectively, as indicated in the figure. This corresponds to the strong interaction region in which the potential energy differs significantly from that of the isolated H_2 and NH molecules.

mechanism. This kind of analysis proved most useful for the study of short-lived collision complexes in the D + H_2 reaction.[125] Generally speaking, the collision time, τ_c, is the time which the three atoms spend close together without possible assignment to any of the three collision channels. A precise definition of the collision time is not exempt from controversy. Perhaps the simplest and most reliable criterion to define this magnitude in classical terms is based on the inspection of the potential. When the three atoms are sufficiently close to each other, the potential is generally distorted with respect to its asymptotic behavior as can be appreciated in Figure 10 for a particular trajectory of the $N(^2D) + H_2$ reaction at 0.165 eV collision energy. It is apparent from the figure that there exists a lapse of time of strong interaction in which the potential is clearly perturbed. A careful examination of trajectories for a given reaction indicates that this generally occurs when the initial, R_{cm}, and final, R'_{cm}, center-of-mass atom−diatom distances are less than two distance parameters R_{int} and R'_{int} which define the strong interaction region. The values of these parameters depend on the reaction and are determined by following the time evolution of the interatomic distances and potential energy for a significant number of trajectories. Usually, $R_{int} = R'_{int} \approx 2-3$ Å. This definition allows a simple determination of the collision time for a given trajectory as[126,127]

$$\tau_{col} = t_{tot} - \frac{\Delta R_{cm}}{v_r} - \frac{\Delta R'_{cm}}{v'_r} \qquad (1)$$

where t_{tot} is the total duration of the trajectory, $\Delta R_{cm} = R_0 - R_{int}$, $R'_{cm} = R_0 - R'_{int}$, R_0 is the initial and final value of the atom−diatom distance, and v_r and v'_r are the initial and final relative velocities. According to eq 1 the collision time would be the time delay between the beginning of the interaction (when the reagents come together at a distance $R_{cm} = R_{int}$) and the formation of products (when $R'_{cm} \geq R'_{int}$). Thus for a hypothetical trajectory in which the formation of the products takes place instantaneously, its collision time would be equal to zero. Obviously, a real trajectory, even the most direct one, will have a finite collision time, implying that there is a delay between the beginning of the interaction and the formation of products.

Notice that this approach makes the recalculation of reactive trajectories to determine τ_{col} unnecessary, and, actually, a more precise determination, carried out by running again the reactive trajectories and monitoring the changes in the potential energy,[125] indicates that the error in the estimation of the collision time based on the values of the initial and final relative distances of interaction is negligible.

Distributions of collision times of reactive trajectories, $P(\tau_c)$, for the four reactions considered in this work are shown in Figure 11. The calculations have been carried out on the ground state PES of the respective reaction and the collision energies corresponding to some of the experiments commented on above. All of the distributions have a similar shape with a relatively sharp rise, a maximum, and then a slow decaying tail, but the differences between the reaction intermediates become apparent in this figure. In the two more exoergic systems, $O(^1D) + H_2$ and $N(^2D) + H_2$, the triatomic complexes are formed with much energy in excess of their dissociation limit and can break apart more easily. The corresponding $P(\tau_c)$ peak at about 100 fs and die away before 500 fs. In contrast, for the two less exoergic systems, $C(^1D) + H_2$ and $S(^1D) + H_2$, the τ_c distributions peak at 200−300 fs are much broader and extend to 5 ps. The lifetimes of the classical complexes in the various reactions are paralleled by the relative widths of the resonance features in the QM reaction probabilities, as mentioned above (see also discussion in ref 68).

More detailed dynamical information can be obtained from the combined distributions of classical collision times and scattering angles, $P(\theta, \tau_{col})$. Three-dimensional representations of these distributions for the more exoergic reactions $O(^1D) + H_2$ and $N(^2D) + H_2$ are shown in Figure 12. As can be seen, the symmetry of the DCSs disappears when the time dimension is added.

The upper panel of this figure shows the distribution of the OH molecules generated in the $O(^1D) + H_2$ ($v = 0$, $j = 0$) reaction at $E_{col} = 56$ meV, which is the collision energy of the experiment of Yang and co-workers.[102,105] All trajectories are of the insertion type as expected, but those at the faster end are not isotropically distributed. The shortest collision times ($\tau_c <$ 60 fs) correspond to forward scattering associated with a rather direct mechanism in which the $O(^1D)$ atom inserts through the bond and carries away one of the hydrogen atoms in the incoming direction. A prominent backward peak with a shoulder is obtained for $\tau_{col} = 80-100$ fs. In this case, the atom also inserts into the bond, but then usually one bending vibration takes place before the OH molecule is ejected in the backward direction. For longer collision times, the distribution becomes gradually more isotropic. Note that the backward structure is still appreciable in the time-integrated DCSs (see Figure 5).

The $P(\theta, \tau_{col})$ for the $N(^2D) + H_2$ reaction at a collision energy of 0.165 eV is represented in the bottom panel of Figure 12. This collision energy corresponds to one of the experiments of Casavecchia and co-workers.[117] In this case, a few fast trajectories ($\tau_{col} <$ 40 fs) of the abstraction type, yielding backward scattering, are found. They correspond to a collinear attack above the $C_{\infty v}$ barrier of the $1^2A''$ ground state surface. Note that this system has a relatively high barrier (0.21 eV) for collinear geometries on the ground state PES. The addition of the zero-point energy (0.27 eV) of the H_2 molecule to the E_{col} considered is enough to surmount this collinear barrier. In the angle−integrated distribution of Figure 11 there is a small distinct peak at the short τ_{col} end, corresponding to abstractive trajectories. An analysis of these trajectories shows that they lead to the highest vibrational excitation ($v' = 3$, $v' = 4$) of the NH molecules, as intuitively expected for head on collisions. The rest of the trajectories are of the insertion type. In analogy with the just mentioned case of $O(^1D) + H_2$, the fastest insertion

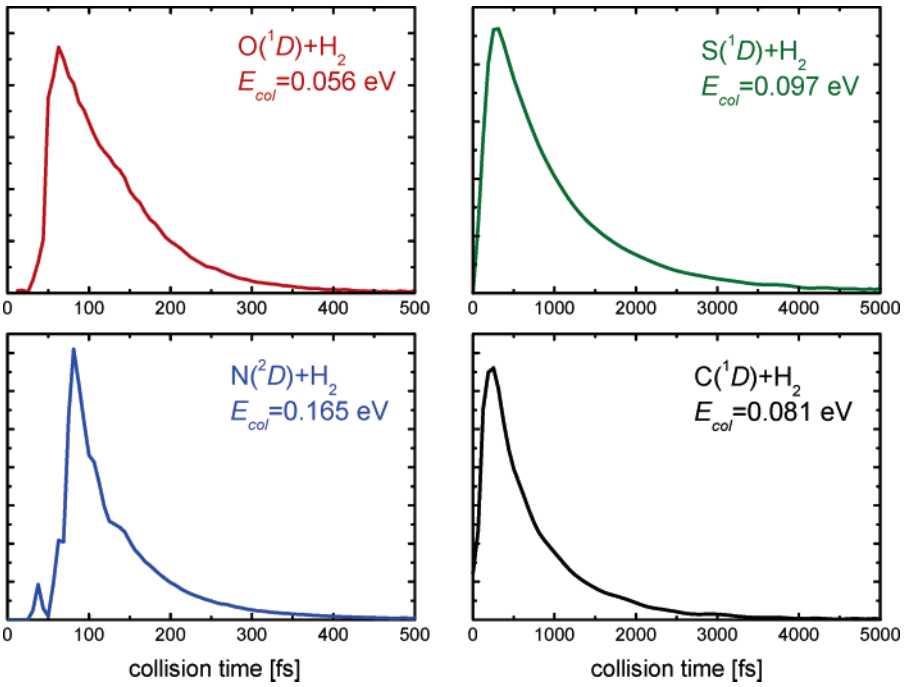

Figure 11. Distribution of collision times, τ_{col}, for the $O(^1D) + H_2$ (upper left), $S(^1D) + H_2$ (upper right), $N(^2D) + H_2$ (lower left), and $C(^1D) + H_2$ (lower right) reactions. Note the difference in the abscissa scales in each case.

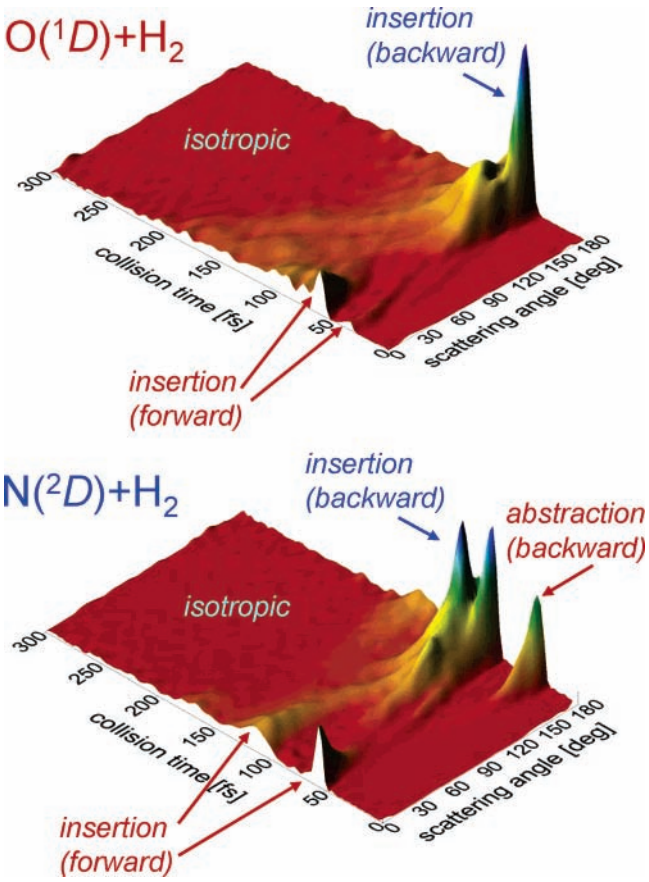

Figure 12. Three-dimensional plots of the combined distribution of collision times and scattering angles for the $O(^1D) + H_2$ (top panel) and $N(^2) + H_2$ (bottom panel) reactions calculated at 56 and 165 meV collision energies, respectively. The features corresponding to different dynamical mechanisms are indicated in the figure.

trajectories give rise to anisotropic angular distributions with alternating forward peaks and large backward peaks, depending on whether a bending vibration occurs or not after the insertion to the H_2 bond. A broad backward shoulder is also observed. Beyond ≈140 fs, the angular distributions become more isotropic displaying a backward−forward symmetry. Figure 13 shows typical trajectories of the abstraction and insertion types just described for the $N(^2D) + H_2$ reaction. [Animation of the trajectories of Figure 13[128] is presented as Supporting Information: S1 (abstraction−backward), S2 (insertion−forward), S3 (insertion−backward), and S4 (long−lived).]

At a given time t after the beginning of the interaction, only those trajectories for which $\tau_{col} < t$ will yield products. Thus, for each of these trajectories, the products will have a time (delay) $t - \tau_{col}$ to fly away such that the center-of-mass (relative) distance of the reaction products will be given at that time by[127]

$$R'_{cm} = v'_r(t - \tau_{col}) + R'_{int} \quad (2)$$

Using this definition of time delay, it is possible to investigate the time evolution of the product scattering generating snapshots, which would be the classical analogs of those produced by Althorpe using wave packet calculations for the $H + D_2$ and $F + HD$ reactions,[129,130] in which the dependence of the DCS with time is portrayed as polar plots in distance and scattering angle, rendering information not only on where and when the products are formed but also how they are scattered in space. The practical implementation of this idea is described in detail in ref 127. Figure 14 shows three-dimensional angle-distance polar maps as a function of time for the $N(^2D) + H_2$ ($v = 0, j = 0$) reaction at a collision energy of 0.165 eV. As can be seen, at short time delays a prominent backward peak appears which is due to abstraction trajectories [left top panel of Figure 13; see also animation S1]. As time evolves, the backward peak starts moving away and a sharp forward peak grows reaching a maximum at a time delay of 58 fs. When the delay time reaches a value of 92 fs, a new peak in backward occurs. These forward and backward peaks appearing in a time interval of 50−100 fs correspond to insertion trajectories with distinct properties. The forward peak is due to insertion trajectories of the type represented in the right top panel of Figure 13 labeled "insertion−forward" in which reaction occurs right after the insertion

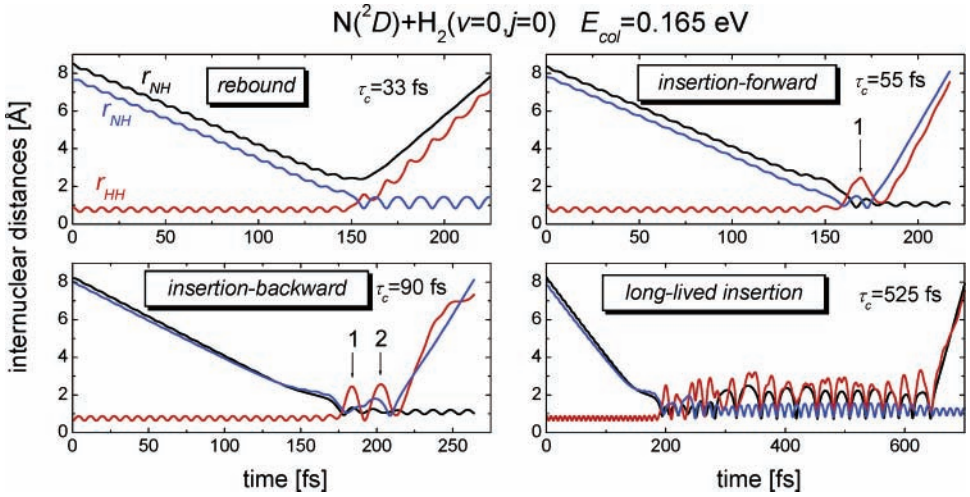

Figure 13. Representation of typical trajectories (internuclear distances as a function of time) with the indicated collision times for the N(^2D) + H_2($v = 0$, $j = 0$) reaction at 165 meV collision energy corresponding to the different dynamical mechanisms of the reaction, labeled as rebound, insertion−forward, insertion−backward, and long-lived insertion (see text for more details).

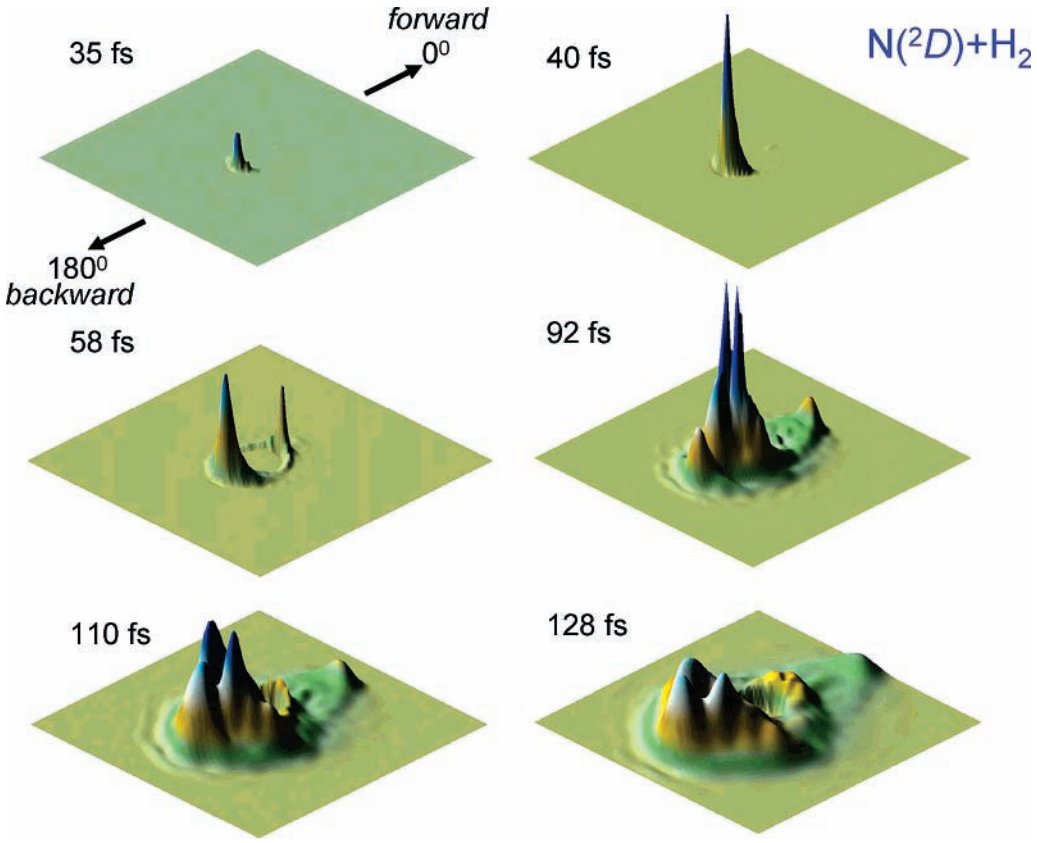

Figure 14. Three-dimensional plots showing the time and spatial evolution of the NH product scattering formed in the N(^2D) + H_2 reaction at 165 meV collision energy. See text for more details. [For the complete animation showing the scattering of the products as a function of time, see Supporting Information S5.]

of the attacking atom into the internuclear axis of the H_2 molecule [animation S2]. However, in the case of the backward peak, the trajectories are as that shown in the left bottom panel of Figure 13 labeled "insertion−backward" [animation S3]. In this case, two insertions (indicated as "1" and "2" in the figure) of the attacking atom through the internuclear axis of the H_2 molecule are produced before reaction takes place. For larger delay times, the distribution becomes more isotropic corresponding to trajectories with long enough collision times as to lose memory of the initial the direction, yielding isotropically scattered products [animation S4]. [The complete evolution of the DCS with time is shown as part of the Supporting Information in animation S5].

The $P(\theta, \tau_{col})$ distributions for the reactions of C(^1D) + H_2 ($v = 0$, $j = 0$) at $E_{col} = 0.08$ eV and of S(^1D) + H_2 ($v = 0$, $j = 0$) at $E_{col} = 0.097$ eV are represented in Figure 15. The energies correspond to those of refs 13 and 51, respectively. For these reactions, all trajectories are of the insertion type. The collision complexes are on average much longer-lived and the angular distribution more isotropic than those of the reactions with O(^1D) and N(^2D). Notwithstanding, anisotropic distributions are also obtained for $\tau_{col} < 100-150$ fs. For collision times

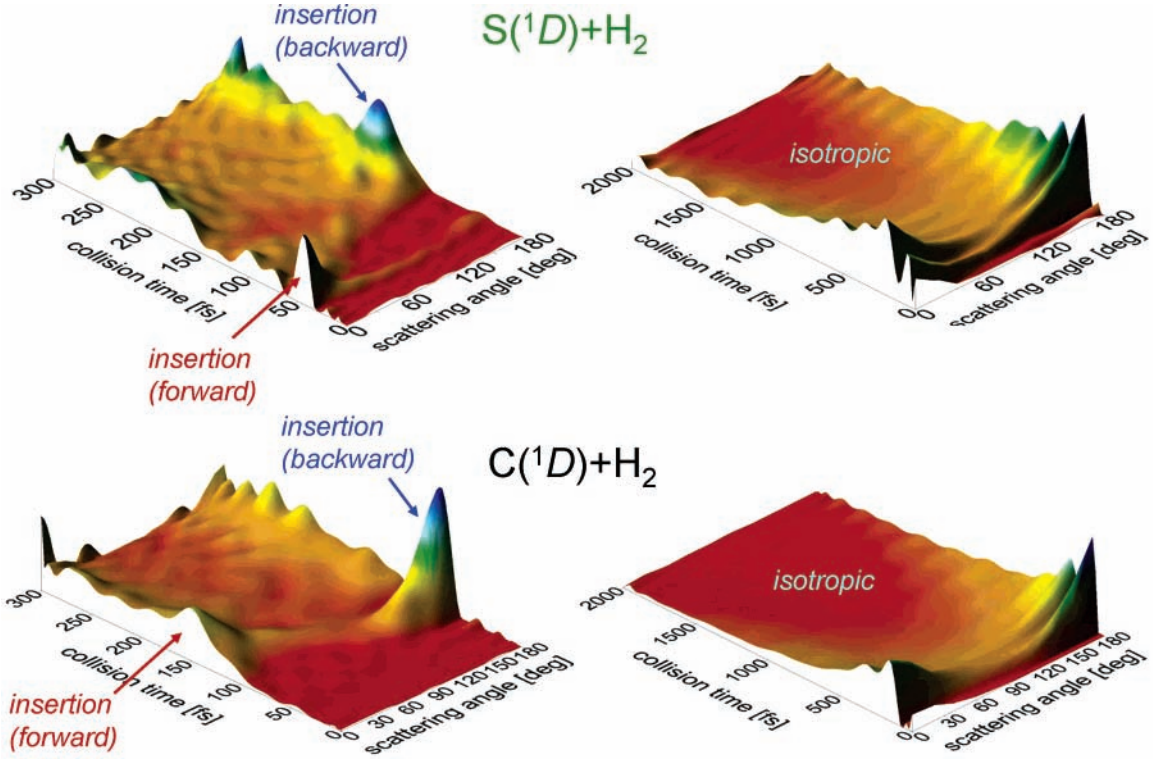

Figure 15. Three-dimensional plots of the total differential cross section as a function of the collision time and scattering angles for the S(^1D) + H_2 (top panel) and C(^{1}) + H_2 (bottom panel) reactions. The features corresponding to different dynamical mechanisms are indicated in the figure. Left panels: collision times in the range $0 \leq \tau_{col} \leq 300$ fs. Right panels: collision times in the range $0 \leq \tau_{col} \leq 2000$ fs.

longer than 200 fs, the angular distributions are essentially isotropic.

The comparison of the $P(\theta, \tau_{col})$ shows that a similar mechanism operates in the shorter time-scale (<100 fs) for the four reactions: insertion collisions give rise to short-lived intermediates of the "osculating complex" type, with lifetimes smaller or comparable to those of the rotation period of the collision complex. For longer times, the insertion complexes formed can vibrate and rotate, lose memory of their initial direction, and randomize the available energy giving rise to statistical distributions. These longer lived collisions dominate largely the more thermoneutral C(^1D) + H_2 and S(^1D) + H_2 reactions.

It is interesting to observe that the calculated lifetime distributions of the various intermediates are within the range of present femtochemistry measurements and invite experimental investigation.

VI. Summary and Outlook

In retrospect, the progress achieved over the past decade in our knowledge of the reactions under consideration has been impressive, taking into account the difficulties associated with rigorous theoretical calculations and with the implementation of experimental techniques that rely on the efficient production of excited metastable atoms. In this period, ab initio potential surfaces of high quality have become available for the four reactions considered, not only for the ground but also for the excited states. An accurate time-independent QM approach, rigorous statistical QM methods, and wavepacket calculations have been successfully applied for the description of the experimental observations. On the experimental side, a large variety of techniques of increasing resolution have been applied, most of them based on the use of crossed molecular beams and lasers. However, it is also true that in spite of the intensive efforts dedicated to the study of the prototypic O(^1D) + H_2, N(^2D) + H_2, C(^1D) + H_2, and S(^1D) + H_2 insertion reactions over the last years, they are not yet so well characterized as their H + H_2 and F + H_2 abstraction counterparts, revealing a much larger degree of complexity.

The results of the previous sections show that, for all of the systems considered, the reaction takes place mostly over the ground state electronic surface, at least for the range of collision energies of the current experiments. Only in the cases of O(^1D) + H_2 and C(^1D) + H_2 is there compelling evidence of the contribution of the 1 $^1A''$ excited-state to the overall reactivity. For the first of these reactions, the participation of 1 $^1A''$ is negligible at collision energies below 0.1 eV. The contribution of the excited PES seems to be more important in the C(^1D) + H_2 reaction since it is barrierless at certain angular configurations, and also has a deep well.

Except for N(^2D) + H_2, all reactions on the ground PES are barrierless for perpendicular insertion and have gas kinetic rate constants. Abstraction collisions only take place over the excited $1^1A''$ surface of O(^1D) + H_2 and to a very small extent on the $1^2A''$ ground state surface of N(^2D) + H_2, which has a relatively low collinear barrier. In the latter case, abstraction collisions are not relevant for the conditions of the presently available experiments.

Insertion collisions form a triatomic reaction intermediate that decomposes giving rise to approximately symmetrical differential cross sections and statistical products' states distributions. The intermediates in the exoergic reactions O(^1D) + H_2 and N(^2D) + H_2 are formed with much energy in excess of their dissociation limit and have an appreciably shorter average lifetime than those form the more thermoneutral C(^1D) + H_2 and S(^1D) + H_2 reactions. As a consequence, the DCSs for O(^1D) + H_2 and N(^2D) + H_2 are less symmetric and their

products' states distributions less statistical than those for the other two reactions.

The QCT method has also been shown to perform extremely well in dynamical calculations from rate constants to differential cross-sections and products' states distributions, especially if one considers its relative simplicity. The use of a Gaussian binning procedure for the assignment of the final energy levels improves significantly the agreement between QCT and QM results. Only some of the QM features, as the experimentally elusive sharp peaks in the DCSs, tentatively attributed to tunneling, are not obtained in the classical calculations (see, however, ref 110).

In the previous sections, it has been shown that the coherent global picture of the dynamics described thus far presents still many open questions worth investigating. There remain discrepancies between experimental results and theoretical calculations. The high-temperature experimental rate coefficients with translationally hot atoms[59,60] for $O(^1D) + H_2$ have not been reproduced in any theoretical calculation, and the room-temperature rate coefficient[84] measured for $S(^1D) + H_2$ is higher than the calculated values.[54,83] These results demand more detailed experiments which can overcome some of their possible limitations. For this same reaction, the predictions of significant electronic quenching due to intersystem crossing[53] have not been verified.

The experimental excitation functions[11,61] for $O(^1D) + H_2$ and for the OD + H channel of $O(^1D) + HD$ seem to rise faster than all theoretical predictions for $E_{col} > 0.1$ eV. Quasiclassical calculations predict an appreciable effect of rotation in the reactivity of the $N(^2D) + H_2$, in contrast with the results of a statistical QM model.[73] For the $S(^1D) + H_2$ system, the measured excitation functions show some differences in shape between the deuterated isotopic variants[49] that are not found in the calculations.[48,54,83]

Traditionally inter- and intramolecular isotopic branching ratios have proved a sensitive probe of chemical mechanisms and of the accuracy of the potential surfaces (see refs 11 and 115 and references therein). These branching ratios have been estimated for the reactions under study both for thermal rate constants and for cross sections.[11] In most cases, some discrepancies appear between measurements and calculations.[12,54,64,73,97]

The present experimental resolution is probably not enough to discern clearly the sharp backward and forward peaks in the QM DCSs. Furthermore, the DCSs calculated with accurate QM methods show apparent discrepancies with the results derived from the highest resolution experiment on $O(^1D) + H_2/HD$[105,106] (see Figure 3), which, interestingly, are in better agreement with QCT calculations. In some cases, the experiments have led to asymmetric DCSs for the $S(^1D) + H_2$ reaction,[51] at variance with theoretical results.[83,126]

There are also some differences worth observing in the products' vibrational populations of $C(^1D) + H_2$[122] and $S(^1D) + H_2$[126] and, most notably, in the rotational states distributions for $N(^2D) + H_2$. In this case, the experimental populations[114,115] are significantly colder than those predicted by the calculations.

Besides the pending clarification of the mentioned discrepancies, there are also promising new approaches, both experimental and theoretical, that may allow dynamical studies with an unprecedented level of detail. In this respect, the investigation of stereodynamical properties[98,99] and of the fine structure components in the states' population of the open-shell product molecules[15,22] should be mentioned.

Higher resolution experiments, like those using the Rydberg tagging technique, applied thus far only to the $O(^1D) + H_2$ and to the $O(^1D) + HD \rightarrow OH + D$ reactions,[28,101−106] might shed much light on the still open dynamical issues.

Acknowledgment. In the course of the last years, we have benefited from the collaboration with many eminent colleagues on this subject: N. Balucani, B. Bussery-Honvault, M. Brouard, P. Casavecchia, J. F. Castillo, M. P. de Miranda, T. Gonzalez-Lezana, T. S. Ho, P. Honvault, J. M. Launay, D. Manolopoulos, M. T. Martínez, B. Martínez-Haya, V. Sáez Rábanos, S. Vaźquez, and X. Yang. To all of them, we express our gratitude for their important contribution to our work on this subject. This work has been funded by the Ministerio de Educación y Ciencia of Spain under Grants CTQ2005-08493-C01-01/BQU (UCM), FIS2004-00456, and FTN2003-08228-C03-03 (CSIC). Financial support from Universidad Complutense-Comunidad de Madrid Grant No. 910729 is also acknowledged. F.J.A. acknowledges the funding by the University Complutense under the program "Sabáticos Complutense" for a sabbatical stay in the University of Oxford. The research was performed within the Unidad Asociada "Química Física Molecular" between the Universidad Complutense and the "Instituto de Estructura de la Materia" (CSIC).

Supporting Information Available: Animation of the trajectories of Figure 13: S1 (abstraction−backward), S2 (insertion−forward), S3 (insertion−backward), S4 (long−lived), and S5. This material is available free of charge via the Internet at http://pubs.acs.org.

References and Notes

(1) Cario, I. G.; Franck, J. *Z. Phys.* **1923**, *17*, 202.
(2) Breckenridge, W. H.; Umemoto, H. The Dynamics of the Excited State. In *Advances in Chemical Physics*; Lawley, K., Ed.; Wiley: New York, 1982; Vol. 50.
(3) Breckenridge, W. H. *J. Phys. Chem.* **1996**, *100*, 14840.
(4) Luntz, A. C.; Schinke, R.; Lester, W. A., Jr.; Günthard, H. H. *J. Chem. Phys.* **1979**, *70*, 5908.
(5) Buss, R. J.; Casavecchia, P.; Hiroka, T.; Sibener, S. J.; Lee, Y. T. *Chem. Phys. Lett.* **1981**, *82*, 386.
(6) Whitlock, P. A.; Muckerman, J. T.; Fisher, E. R. *J. Chem. Phys.* **1982**, *76*, 4468.
(7) Polák, R.; Paiderová, I.; Kuntz, P. J. *J. Chem. Phys.* **1987**, *87*, 2863.
(8) Kuntz, P. J.; Niefer, B. I.; Sloan, J. J. *J. Chem. Phys.* **1988**, *88*, 3629.
(9) Kuntz, P. J.; Niefer, B. I.; Sloan, J. *J. Chem. Phys.* **1991**, *151*, 77.
(10) Casavecchia, P. *Rep. Prog. Phys.* **2000**, *63*, 335.
(11) Liu, K. *Int. Rev. Phys. Chem.* **2001**, *20*, 189.
(12) Aoiz, F. J.; Bañares, L.; Brouard, M.; Castillo, F. J.; Herrero, V. J. *J. Chem. Phys.* **2000**, *113*, 5339.
(13) Bergeat, A.; Cartechini, L.; Balucani, N.; Capozza, G.; Phillips, L. F.; Casavecchia, P.; Volpi, G. G.; Bonnet, L.; Rayez, J.-C. *Chem. Phys. Lett.* **2000**, *327*, 197.
(14) Balucani, N.; Alagia, M.; Cartechini, L.; Casavechia, P.; Volpi, G. G.; Pederson, L. A.; Schatz, G. C. *J. Phys. Chem.* **2001**, *105*, 2414.
(15) Khachatrian, A.; Dagdigian, P. J. *J. Chem. Phys.* **2005**, *122*, 024303.
(16) Durand, G.; Chapuisat, X. *Chem. Phys.* **1985**, *96*, 381.
(17) Walch, S. P.; Harding, L. B. *J. Chem. Phys.* **1988**, *88*, 7653.
(18) Drukker, K.; Schatz, G. C. *J. Chem. Phys.* **1999**, *111*, 2451.
(19) Gray, K. S.; Petrongolo, C.; Drukker, K.; Schatz, G. C. *J. Phys. Chem. A* **1999**, *103*, 9448.
(20) Hoffmann, M. R.; Schatz, C. G. *J. Chem. Phys.* **2000**, *113*, 9456.
(21) Maiti, B.; Schatz, G. C. *J. Chem. Phys.* **2003**, *119* 12360.
(22) Alexander, M. H.; Rackham, E. J.; Manolopoulos, D. E. *J. Chem. Phys.* **2004**, *121*, 5221.
(23) Ho, T.-S.; Hollebeck, T.; Rabitz, H.; Harding, L. B.; Schatz, G. C. *J. Chem. Phys.* **1996**, *105*, 10472.
(24) Schatz, G. C.; Papaioannou, A.; Pederson, L. A.; Harding, L. B.; Hollebeck, T.; Ho, T.-S.; Rabitz, H. *J. Chem. Phys.* **1997**, *107*, 2340.
(25) Schinke, R.; Lester, W. A., Jr. *J. Chem. Phys.* **1980**, *72*, 3754.
(26) Dobbyn, A. J.; Knowles, P. J. *Mol. Phys.* **1997**, *91*, 1107.
(27) Dobbyn, A. J.; Knowles, P. J. *Farady Discuss.* **1998**, *110*, 247.
(28) Gray, S. K.; Balint-Kurti, G. G.; Schatz, G. C.; Lin, J. J.; Liu, X.; Harich, S.; Yang, X. *J. Chem. Phys.* **2000**, *113*, 7330.

(29) Varandas, A. J. C. *J. Chem. Phys.* **1996**, *105*, 3524; **1997**, *107*, 5987; **1997**, *107*, 867.
(30) Brandão, J.; Rio, C. M. A. *J. Chem. Phys.* **2003**, *119*, 3148.
(31) Pederson, L. A.; Schatz, G. C.; Ho, T.-S.; Hollebeek, T.; Rabitz, H.; Harding, L. B.; Lendvay, G. *J. Chem. Phys.* **1999**, *110*, 9091.
(32) Kobayashi, H.; Takayanagi, T.; Yokohama, K.; Sato, T.; Tsunashima, S. *J. Chem. Soc. Faraday Trans.* **1995**, *91*, 3771.
(33) Kobayashi, H.; Takayanagi, T.; Tsunashima, S. *Chem. Phys. Lett.* **1997**, *91*, 3771.
(34) Pederson, L. A.; Schatz, G. C.; Hollebeek, T.; Ho, T.-S.; Rabitz, H.; Harding, L. B. *J. Phys. Chem. A* **2000**, *104*, 2301.
(35) Santoro, F.; Petrongolo, C.; Schatz, G. C. *J. Phys. Chem. A* **2002**, *106*, 8276.
(36) Ho, T. S.; Rabitz, H.; Aoiz, F. J.; Bañares, L.; Vázquez, S. A.; Harding, L. B. *J. Chem. Phys.* **2003**, *119*, 3063.
(37) Varandas, A. J. C.; Poveda, I. A. *Theor. Chem. Acc.* **2006** online.
(38) Chu, T.-S.; Han, K.-L.; Varandas, A. J. C. *J. Phys. Chem. A* **2006**, *110*, 1666.
(39) Qu, Z.-W.; Zhu, H.; Schinke, R.; Adam, L.; Hack, W. *J. Chem. Phys.* **2005**, *122*, 204313.
(40) Bussery-Honvault, B.; Honvault, P.; Launay, J.-M. *J. Chem. Phys.* **2001**, *115*, 10701.
(41) Bañares, L.; Aoiz, F. J.; Honvault, P.; Bussery-Honvault, B.; Launay, J.-M. *J. Chem. Phys.* **2003**, *118*, 565.
(42) Bañares, L.; Aoiz, F. J.; Vázquez, S. A.; Ho, T.-S.; Rabitz, H. *Chem. Phys. Lett.* **2003**, *374*, 243.
(43) Bussery-Honvault, B.; Julien, J.; Honvault, P.; Launay, J.-M. *Phys. Chem. Chem. Phys.* **2005**, *7*, 1476.
(44) Honvault, P.; Bussery-Honvault, B.; Launay, J.-M.; Aoiz, F. J.; Bañares, L. *J. Chem. Phys.* **2006**, *124*, 154314.
(45) Van Harrevelt, R.; Van Hemert, M. C.; Schatz, G. C. *J. Chem. Phys.* **2002**, *116*, 6002.
(46) Guadagnini, R.; Schatz, C. G. *J. Phys. Chem.* **1996**, *100*, 18944.
(47) Zyubin, A. S.; Mebel, A. M.; Chao, S. D.; Skodje, R. T. *J. Chem. Phys.* **2001**, *114*, 320.
(48) Chao, S. D.; Skodje, R. T. *J. Phys. Chem. A* **2001**, *105*, 2474.
(49) Lee, S.-H.; Liu, K. *Chem. Phys. Lett.* **1998**, *290*, 323.
(50) Lee, S.-H.; Liu, K. *J. Phys. Chem. A.* **1998**, *102*, 8637.
(51) Lee, S.-H.; Liu, K. *Appl. Phys. B.* **2000**, *71*, 627.
(52) Ho, T.-S.; Hollebeck, T.; Rabitz, H.; Chao, S. D.; Skodje, R. T.; Zyubin, A. S.; Mebel, A. M. *J. Chem. Phys.* **2002**, *116*, 4124.
(53) Maiti, B.; Schatz, G. C.; Lendvay, G. *J. Phys. Chem. A* **2004**, *108*, 8772.
(54) Bañares, L.; Castillo, J. F.; Honvault, P.; Launay, J.-M. *Phy. Chem. Chem. Phys.* **2005**, *7*, 627.
(55) Honvault, P.; Launay, J. M. *J. Chem. Phys.* **1999**, *111*, 6665.
(56) Honvault, P.; Launay, J. M. *J. Chem. Phys.* **2001**, *114*, 1057.
(57) Honvault, P.; Launay, J. M. *Chem. Phys. Lett.* **2003**, *370*, 371.
(58) Talukdar, R. K.; Ravishankara, A. R. *Chem. Phys. Lett.* **1996**, *253*, 177.
(59) Koppe, S.; Laurent, T.; Naik, P. D.; Volpp, H.-R.; Wolfrum, J.; Arusi-Parpar, T.; Bar, I.; Rosenwaks, S. *Chem. Phys. Lett.* **1993**, *214*, 546.
(60) Laurent, T.; Naik, P. D., Volpp, H.-R.; Wolfrum, J.; Arusi-Parpar, T.; Bar, I.; Rosenwaks, S. *Chem. Phys. Lett.* **1995**, *236*, 343.
(61) Hsu, Y.-T.; Wang, J.-H.; Liu, K. *J. Chem. Phys.* **1997**, *107*, 2351.
(62) Gray, S. K.; Goldfield, E. M.; Schatz, G. C.; Balint-Kurti, G. G. *Phys. Chem. Chem. Phys.* **1999**, *1*, 1141.
(63) Alexander, A. J.; Aoiz, F. J.; Bañares, L.; Brouard, M.; Herrero, V. J.; Simons, J. P. *Chem. Phys. Lett.* **1997**, *278*, 313.
(64) Lin, S. Y.; Guo, H. *Chem. Phys. Lett.* **2004**, *385*, 193.
(65) Varandas, A. J. C.; Voronin, A. I., Riganelli, A.; Caridade, P. J. S. B. *Chem. Phys. Lett.* **1997**, *278*, 325.
(66) Hankel, M.; Balint-Kurti, G. C.; Gray, S. K.; *J. Phys. Chem. A* **2001**, *105*, 2330.
(67) Rackham, E. J.; Huarte-Larrañaga, F.; Manolopoulos, D. E.; *Chem. Phys. Lett.* **2001**, *343*, 356.
(68) Rackham, E. J.; González−Lezana, T.; Manolopoulos, D. E. *J. Chem. Phys.* **2003**, *119*, 12895.
(69) Lee, S.-H.; Liu, K. *J. Chem. Phys.* **1999**, *111*, 4351.
(70) Suzuki, T.; Shihira, Y.; Dato, T.; Umemoto, H.; Tsunashima, S. *J. Chem. Soc. Faraday Trans.* **1993**, *89*, 995.
(71) Herron, J. T. *J. Chem. Phys. Ref. Data* **1999**, *28*, 1453.
(72) Balucani, N.; Cartechini, L.; Capozza, G.; Segoloni, E.; Casavecchia, P.; Volpi, G. G.; Aoiz, F. J.; Bañares, L.; Honvault, P.; Launay, J. M. *Phys. Rev. Lett.* **2002**, *89*, 013201.
(73) Bañares, L.; Aoiz, F. J.; González-Lezana, T.; Herrero, V. J.; Tanarro, I. *J. Chem. Phys.* **2005**, *123*, 224301.
(74) Lin, S.-Y.; Guo, H. *J. Chem. Phys.* **2006**, *124*, 031101.
(75) Defazio, P.; Petrongolo, C. *J. Chem. Phys.* **2006**, *125*, 064308.
(76) Aoiz, F. J.; Bañares, L.; Herrero, V. J.; Saez Rabanos, V.; Stark, K.; Tanarro, I.; Werner, H.-J. *Chem. Phys. Lett.* **1996**, *262*, 175.
(77) Zhang, D. H.; Lee, S.-Y.; Baer, M. *J. Chem. Phys.* **2000**, *112*, 9802.
(78) Sato, K.; Ishida, N.; Kurakata, T.; Iwasaki, A.; Tsuneyuki, S. *Chem. Phys.* **1998**, *237*, 195.
(79) Lin, S. Y.; Guo, H. *J. Chem. Phys.* **2004**, *120*, 9907.
(80) Lin, S. Y.; Guo, H. *J. Phys. Chem. A* **2004**, *108*, 10066.
(81) Lin, S. Y.; Guo, H. *J. Chem. Phys.* **2004**, *121*, 1285.
(82) Lin, S. Y.; Guo, H. *J. Phys. Chem. A* **2004**, *108*, 2141.
(83) Lin, S. Y.; Guo, H. *J. Chem. Phys.* **2005**, *122*, 074304.
(84) Black, G.; Jusinski *J. Chem. Phys.* **1985**, *82*, 789.
(85) Inagaki, Y.; Shamsuddin, S. M.; Matsumi, Y.; Kawasaki, M. *Laser Chem.* **1994**, *14*, 235.
(86) Butler, J. E.; McDonald, R. G.; Donaldson, D. J.; Sloan, J. J. *Chem. Phys. Lett.* **1983**, *95*, 183.
(87) Butler, J. E.; Jurisch, G. M.; Watson, I. A.; Wiesenfeld, J. R. *J. Chem. Phys.* **1986**, *84*, 5365.
(88) Alexander, A. J.; Blunt, D. A.; Brouard, M.; Simons, J. P.; Aoiz, F. J.; Bañares, L.; Fujimura, Y.; Tsubouchi, M. *Faraday Discuss.* **1997**, *108*, 375.
(89) Alexander, A. J.; Aoiz, F. J.; Bañares, L.; Brouard, M.; Short, J.; Simons, J. P. *J. Phys. Chem. A* **1997**, *101*, 7544.
(90) Che, D.-C.; Liu, K. *J. Chem. Phys.* **1995**, *103*, 5164.
(91) Hsu, Y.-T.; Liu, K. *J. Chem. Phys.* **1997**, *107*, 1664.
(92) Hsu, Y.-T.; Liu, K.; Pederson, L. A.; Schatz, G. C. *J. Chem. Phys.* **1999**, *111*, 7921; **1999**, *111*, 7931.
(93) Hermine, P.; Hsu, Y.-T.; Liu, K. *Phys. Chem. Chem. Phys.* **2000**, *2*, 581.
(94) Alagia, M.; Balucani, N.; Cartechini, L.; Casavecchia, P.; van Kleef, E. H.; Volpi, G. G.; Kuntz, P. J.; Sloan, J. J. *J. Chem. Phys.* **1998**, *108*, 6698.
(95) Casavecchia, P.; Balucani, N.; Alagia, M.; Cartechini, L.; Volpi, G. G. *Acc. Chem. Res.* **1999**, *32*, 503.
(96) Ahmed, M.; Peterka, D. S.; Suits, A. G. *Chem. Phys. Lett.* **1999**, *301*, 372.
(97) Aoiz, F. J.; Bañares, L.; Herrero, V. J. *Chem. Phys. Lett.* **1999**, *310*, 277.
(98) Aoiz, F. J.; Bañares, L.; Castillo, J. F.; Martinez-Haya, B.; Miranda, M. P. *J. Chem. Phys.* **2001**, *114*, 8328.
(99) Aoiz, F. J.; Bañares, L.; Castillo, J.; Brouard, M.; Denzer, W.; Valance, C.; Honvault, P.; Launay, J. M., Dobbin, A.; Knowles, P. *Phys. Rev. Lett.* **2001**, *86*, 1729.
(100) Aoiz, F. J.; Brouard, M.; Enríquez, P. A. *J. Chem. Phys.* **1996**, *105*, 4964.
(101) Liu, X.; Lin, J. J.; Harich, S.; Yang, X. *J. Chem. Phys.* **2000**, *113*, 1325.
(102) Liu, X.; Lin, J. J.; Harich, S.; Schatz, G. C.; Yang, X. *Science* **2000**, *289*, 1536.
(103) Liu, X.; Lin, J. J.; Harich, S.; Yang, X. *Phys. Rev. Lett.* **2001**, *86*, 408.
(104) Liu, X.; Wang, C. C.; Harich, S. A.; Yang, X. *Phys. Rev. Lett.* **2002**, *89*, 133201.
(105) Aoiz, F. J.; Bañares, L.; Castillo, J. F.;Herrero, V. J.; Mart′inez-Haya, B.; Honvault, P.; Launay, J. M.; Liu, X.; Lin, J. J.; Harich, S. A.; Wang, C. C.; Yang, X. *J. Chem. Phys.* **2002**, *116*, 10692.
(106) Yuan, K.; Cheng, Y.; Liu, X.; Harich, S. A.; Yang, X.; Zhang, D.-H. *Phys. Rev. Lett.* **2006**, *96*, 103202.
(107) Schnieder, W.; Meier, W.; Wrede, E.; Welge, K. H.; Ashfold, M. N. R.; Western, C. *J. Chem. Phys.* **1990**, *92*, 7027.
(108) Schnieder, W.; Seekamp−Rahn, K.; Wrede, E.; Welge, K. H. *J. Chem. Phys.* **1997**, *107*, 6175.
(109) Balucani, N.; Casavecchia, P.; Aoiz, F.; Bañares, L.; Castillo, J. F.; Herrero, V. *J. Mol. Phys.* **2005**, *103*, 1703.
(110) Bonnet, L.; Larrégaray, P.; Rayez, J.-C.; González Lezama, T. *Phys. Chem. Chem. Phys.* **2006**, *8*, 3951.
(111) Aoiz, F. J.; Bañares, L.; Castillo, J. F.; Herrero, V. J.; Martínez-Haya, B. *Phys. Chem. Chem. Phys.* **2002**, *4*, 4379.
(112) Mikulecky, K.; Gericke, K.-H. *J. Chem. Phys.* **1992**, *96*, 7490.
(113) Umemoto, H.; Matsumoto, K. *J. Chem. Phys.* **1996**, *104*, 9640.
(114) Umemoto, H.; Asai, T.; Kimura, Y. *J. Chem. Phys.* **1997**, *106*, 4985.
(115) Umemoto, H. *Chem. Phys. Lett.* **1998**, *292*, 594.
(116) Umemoto, H.; Terada, N.; Tanaka, K. *J. Chem. Phys.* **2000**, *112*, 5762.
(117) Alagia, M.; Balucani, N.; Cartechini, L.; Casavecchia, P.; Volpi, G.; Pederson, L. A.; Schatz, G. C.; Lendvay, G.; Harding, L. B.; Hollebeek, T.; Ho, T.-S.; Rabitz, H. *J. Chem. Phys.* **1999**, *110*, 8857.
(118) Balucani, N.; Casavecchia, P.; Bañares, L.; Aoiz, F. J.; Honvault, P.; Launay, J. M. *J. Phys. Chem. A* **2006**, *110*, 817.
(119) Fisher, W. H.; Carrington, T.; Sadowski, C. M.; Dugan, C. H. *Chem. Phys.* **1985**, *97*, 433.
(120) Mikulecky, K.; Gericke, K.-H. *J. Chem. Phys.* **1993**, *98*, 1244.
(121) Balucani, N.; Capozza, G.; Cartechini, L.; Bergeat, A.; Bobbenkamp, R.; Casavecchia, P.; Aoiz, F. J.; Bañares, L.; Honvault, P.; Bussery-Honvault, B.; Launay, J.-M. *Phys. Chem. Chem. Phys.* **2004**, *6*, 4957.

(122) Balucani, N.; Capozza, G.; Segoloni, E.; Russo, A.; Bobbenkamp, R.; Casavecchia, P.; González-Lezana, T.; Rackham, E. J.; Bañares, L.; Aoiz, F. J. *J. Chem. Phys.* **2005**, *122*, 234309.
(123) Aoiz, F. J.; Bañares, L.; Herrero, V. J. *Int. Rev. Phys. Chem.* **2005**, *24*, 119.
(124) Bonnet, L.; Rayez, J. C. *Chem. Phys. Lett.* **1997**, *277*, 183.
(125) Aoiz, F. J.; Herrero, V. J.; Sáez Rábanos, V. *J. Chem. Phys.* **1992**, *97*, 7423.
(126) Bañares, L.; Aoiz, F. J.; Honvault, P.; Launay, J.-M. *J. Phys. Chem. A* **2004**, *108*, 1616.
(127) Martínez, M. T.; Hernández, M. L.; Alvariño, J. M.; Aoiz, F. J.; Sáez Rábanos, V. *J. Chem. Phys.* **2003**, *119*, 7871.
(128) Laaksonen, L. gOpenMol v.3. Espoo, Finland 2005 (available at http://www.csc.fi/gopenmol/).
(129) Althorpe, S. A. *J. Chem. Phys.* **2002**, *117*, 4623.
(130) Althorpe, S. A. *J. Phys. Chem. A* **2003**, *108*, 7152.